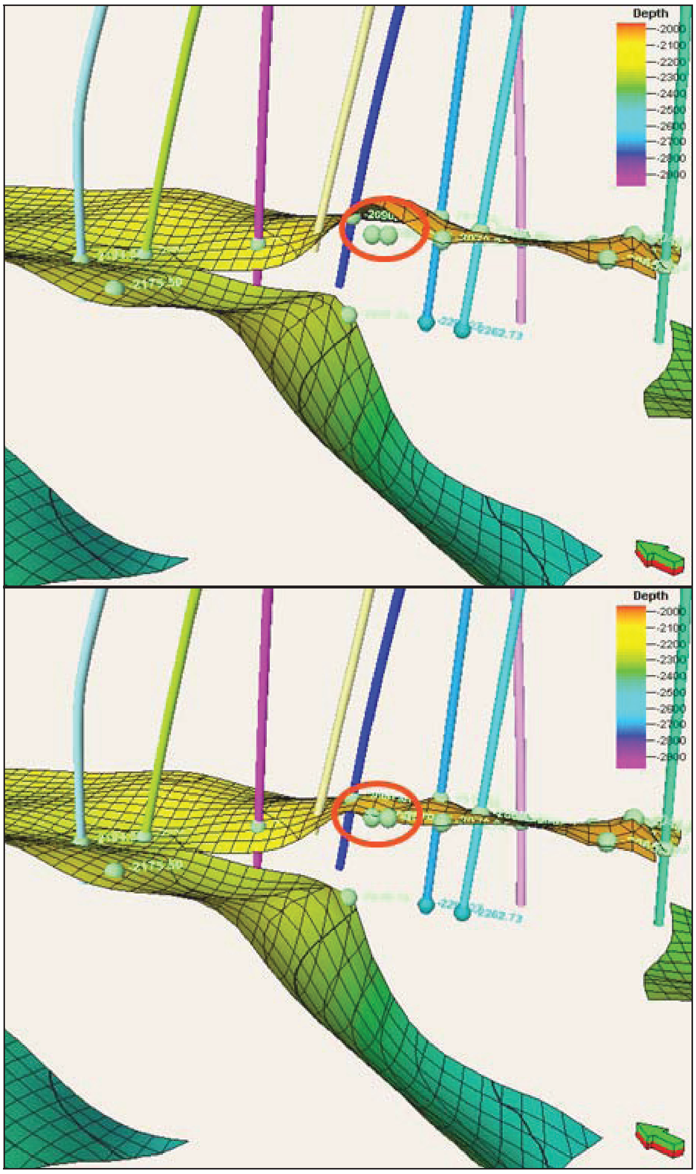

Figure 4-16 Example 1 of the horizon distortion in the Bergermeer Field
Left picture shows the horizon before using the help data points. It shows the undulation on the surface of the Top ROSLU. Help data points #71 and #72 (red circle) helped to constrain the Top ROSLU.

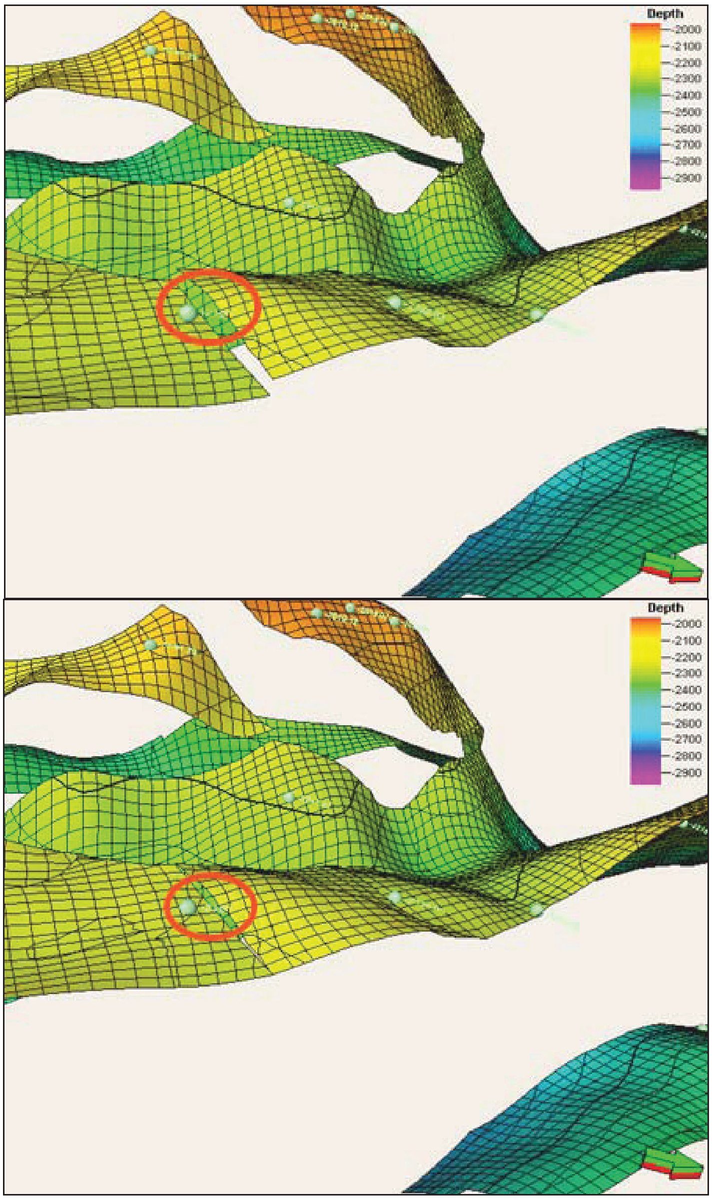

Figure 4-17 **Example 2 of the Horizon distorting in the Bergermeer Field**
Saddle area between Bergermeer and Groet shows fault 7 and fault 20 creating big offset which is not true based on the input data (seismic data of the Top Rotliegend). Help data point #82 (red circle) helped to constrain fault offset according to the available input data.

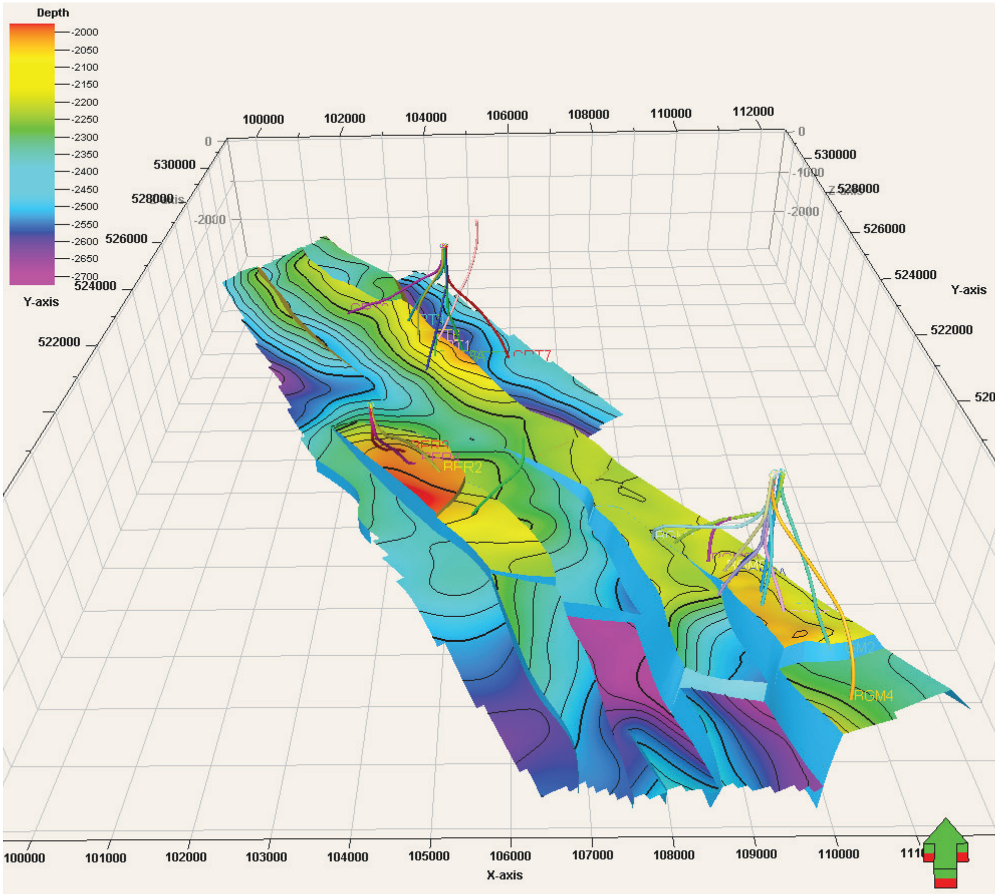

Figure 4-18 **Resulting base case Top ROSLU horizon**

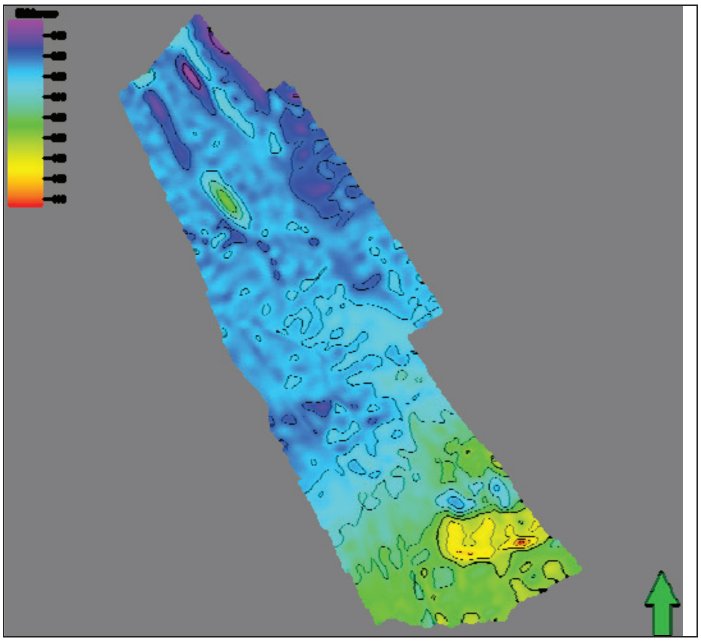

Figure 4-19 **Output (isochore) map based on base case scenario Top ROSLU and Top DCCR.**

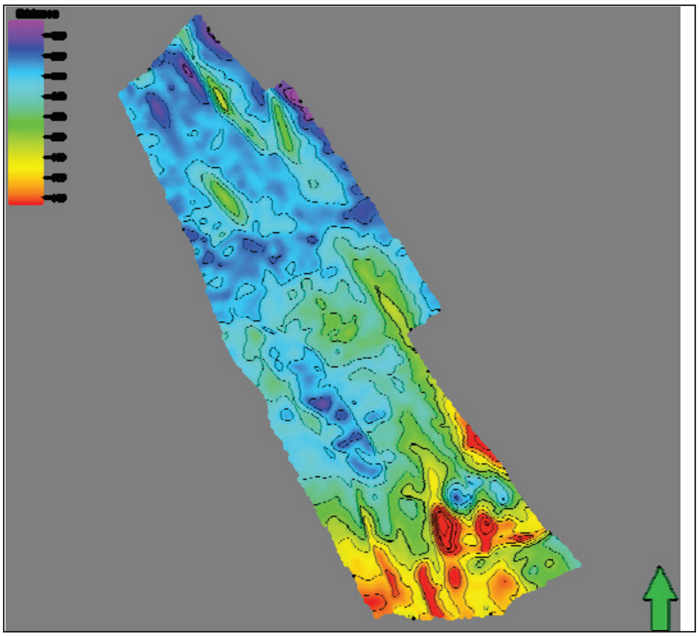

Figure 4-20 **Output (isochore) map based on *low* case scenario Top ROSLU and Top DCCR.**

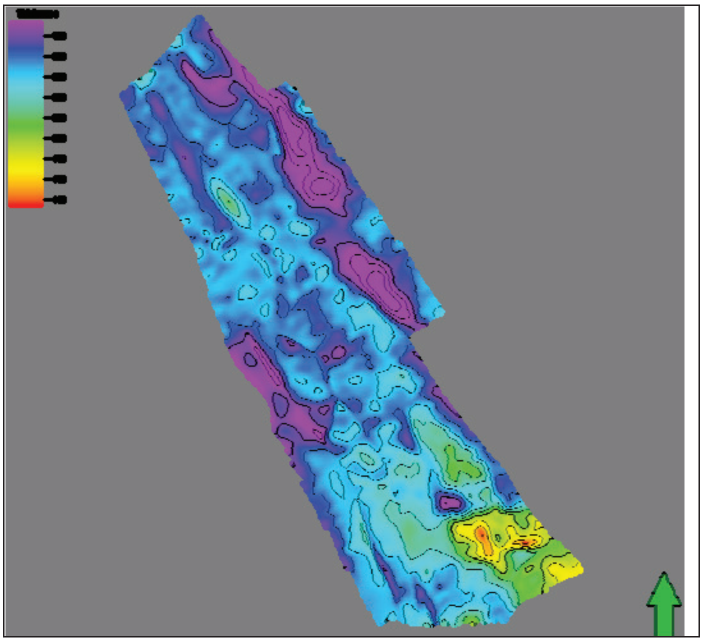

Figure 4-21 **Output (isochore) map based on *high* case scenario Top ROSLU and Top DCCR.**

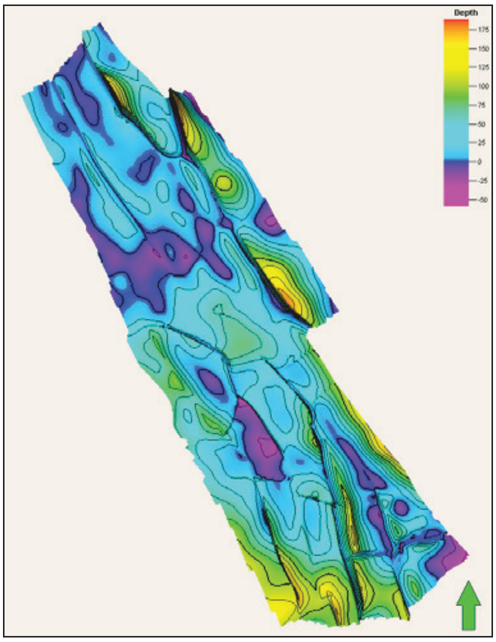

Figure 4-22 **Difference thickness between High and Low case 3D grid Model**

Zero value mainly due to both horizons (high and low case) had to be tied up to the well tops (difference in the well should be zero). Others, zero value also created due to uncertainty map have no correction (refer to Figure 4-12). Negative value as result of changing the input data (uncertainty map) but still use the same well top for both cases.

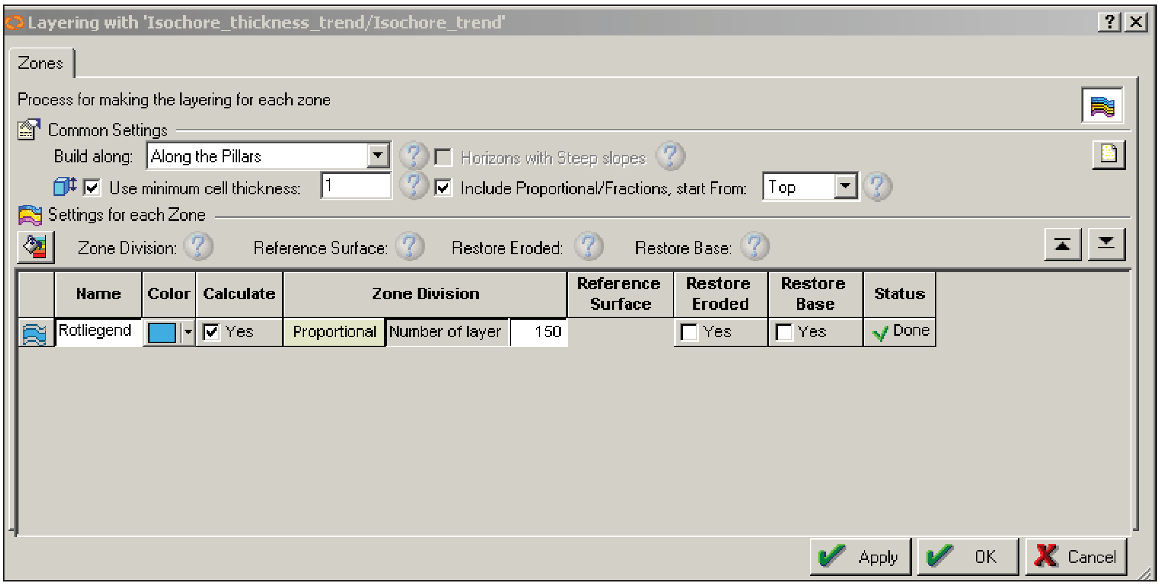

Figure 4-23, **Layering dialogue in the modelling area**

Layering in the project area mainly to captures the thinnest tight streaks porosity. The layering scheme is "proportional to top" and build along the pillars was chosen, and some 150 layers with an average 1.58 meters thickness each generated.

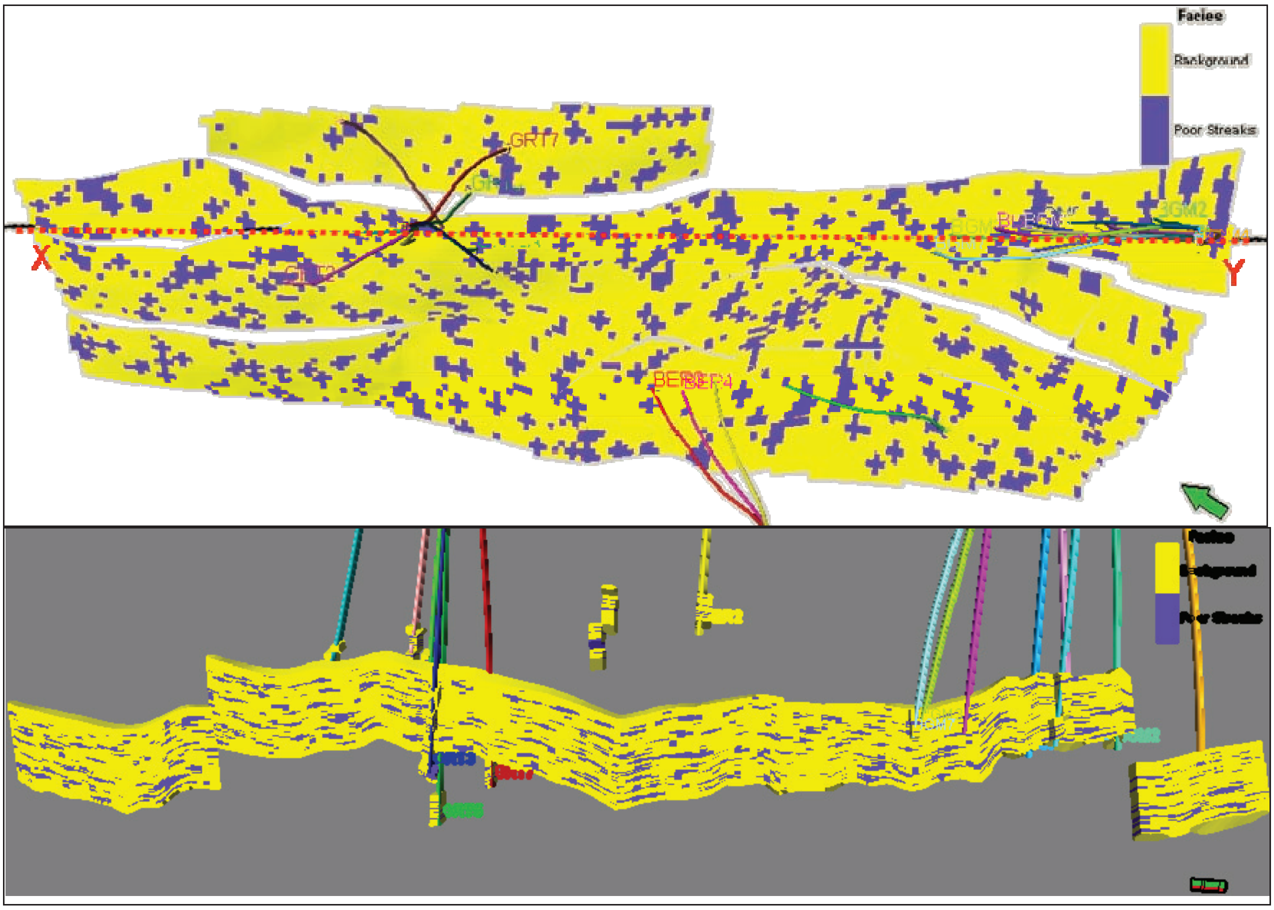

Figure 4-24 **Discontinuous low porosity streaks facies scenario, base case (3D grid without uncertainty map) in the modelling area**
K-layer=79 (up) and I-layer=39 (below). X-Y: cross section for I-layer.

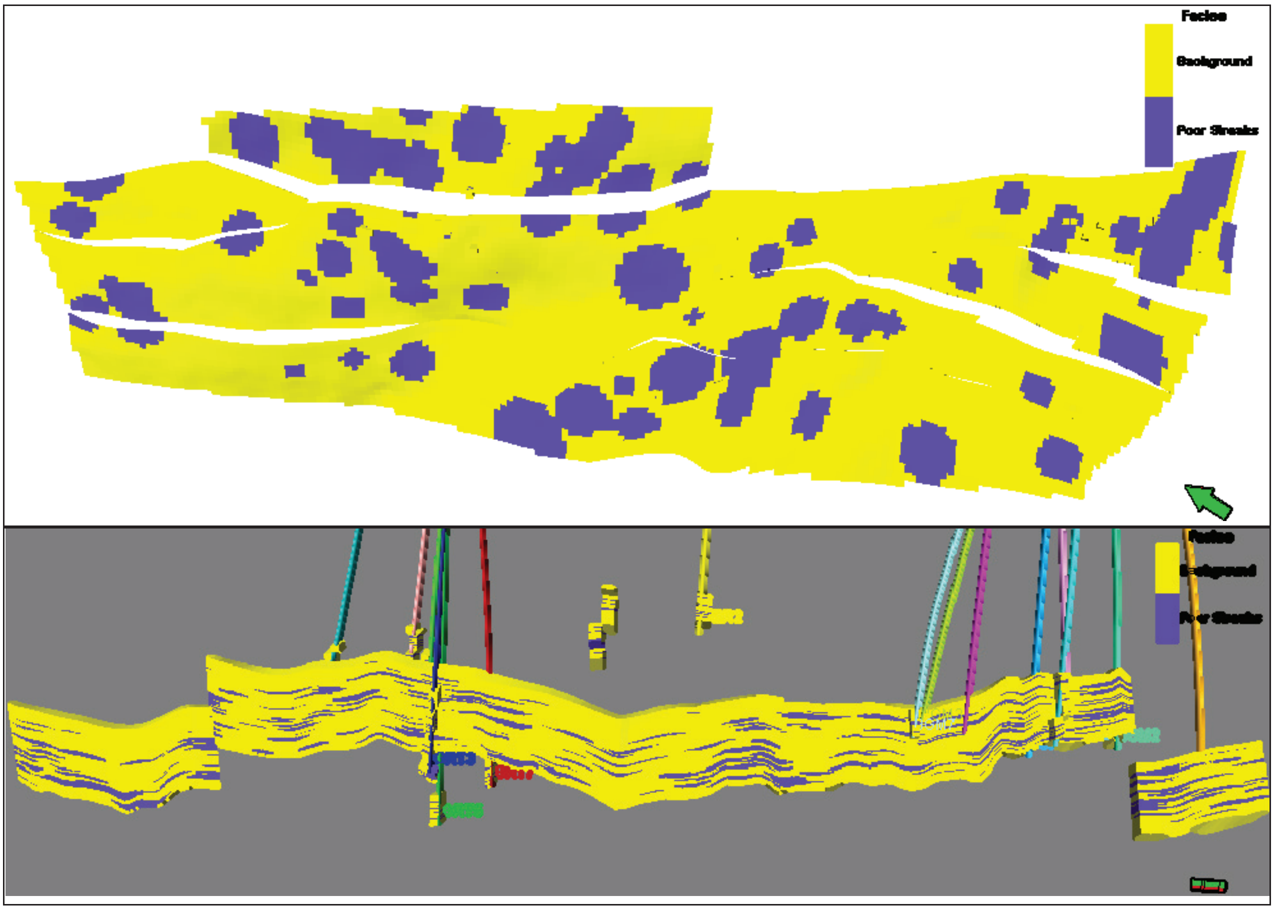

Figure 4-25 **Mid low porosity streaks facies scenario, base case (3D grid without uncertainty map) in the modelling area**
K-layer=79 (up) and I-layer=39 (below)

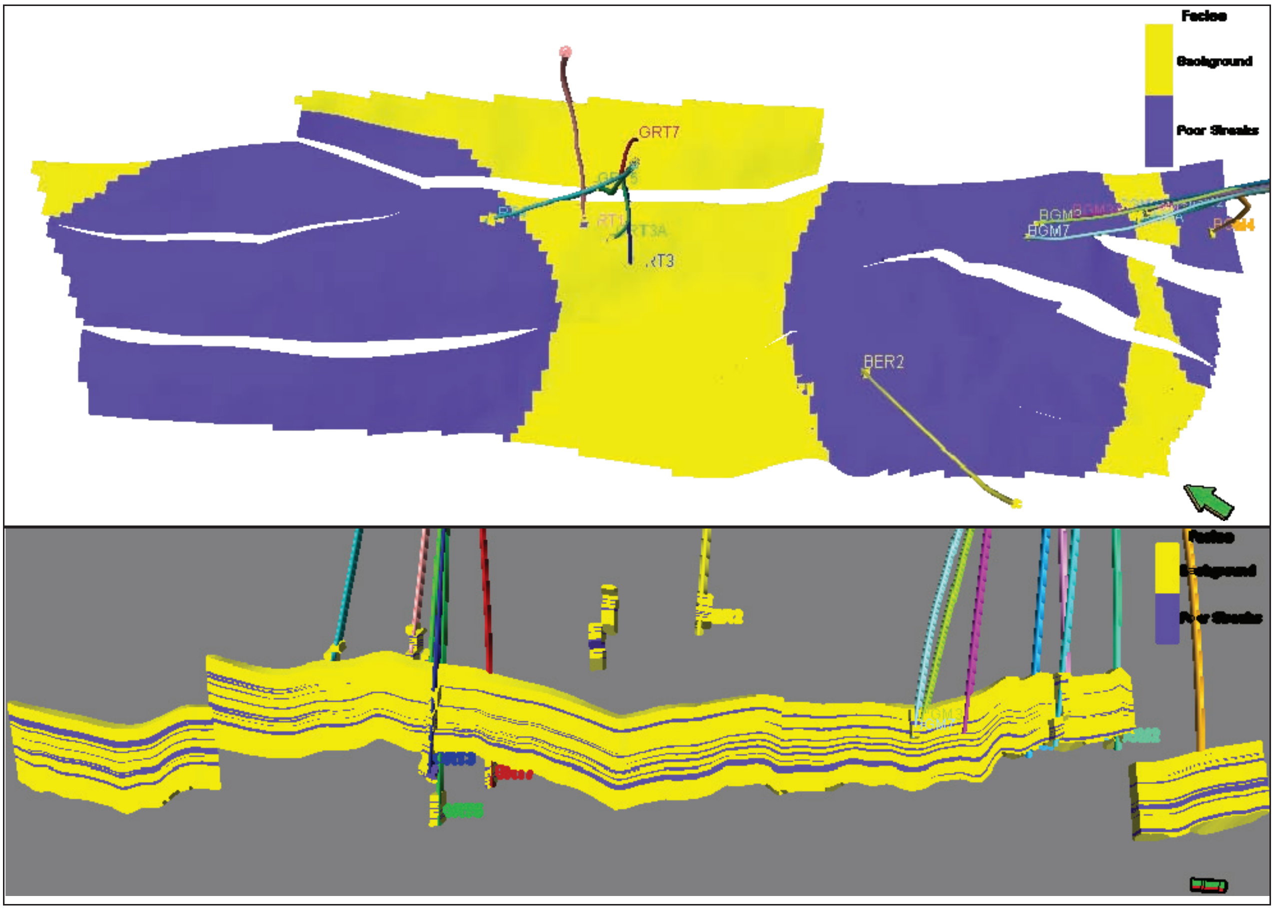

Figure 4-26 Continuous low porosity streaks facies scenario, base case (3D grid without uncertainty map) in the modelling area
K-layer=79 (up) and I-layer=39 (below)

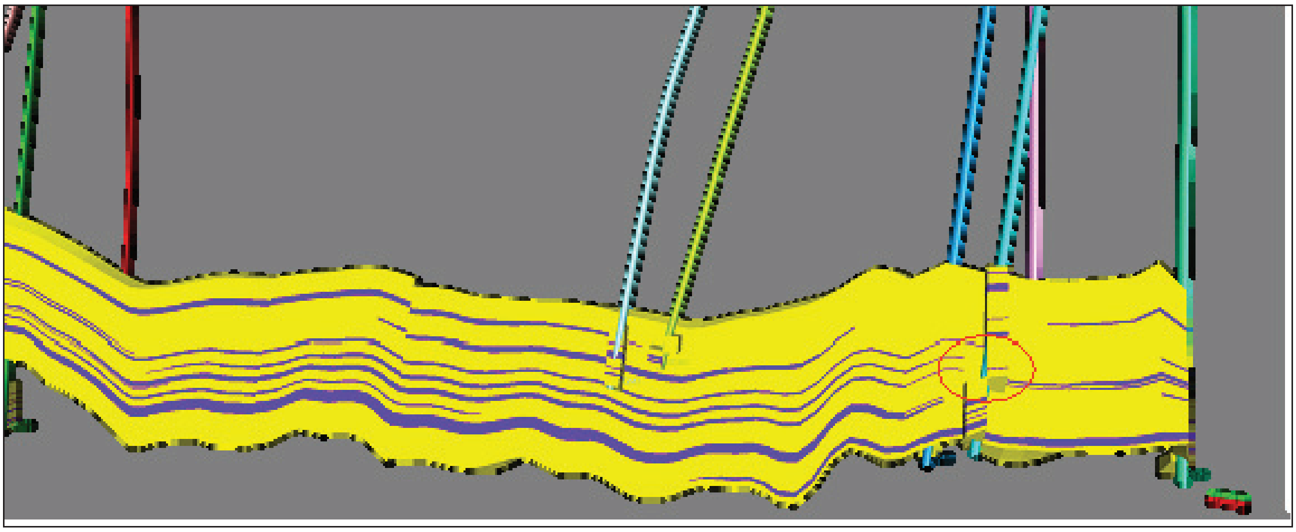

Figure 4-27 **Cross-section of the 'continuous' case, with highlighted upscaled well cells, showing that we are overestimating the lateral range of the poor streaks (purple) in this case (see red circle).**

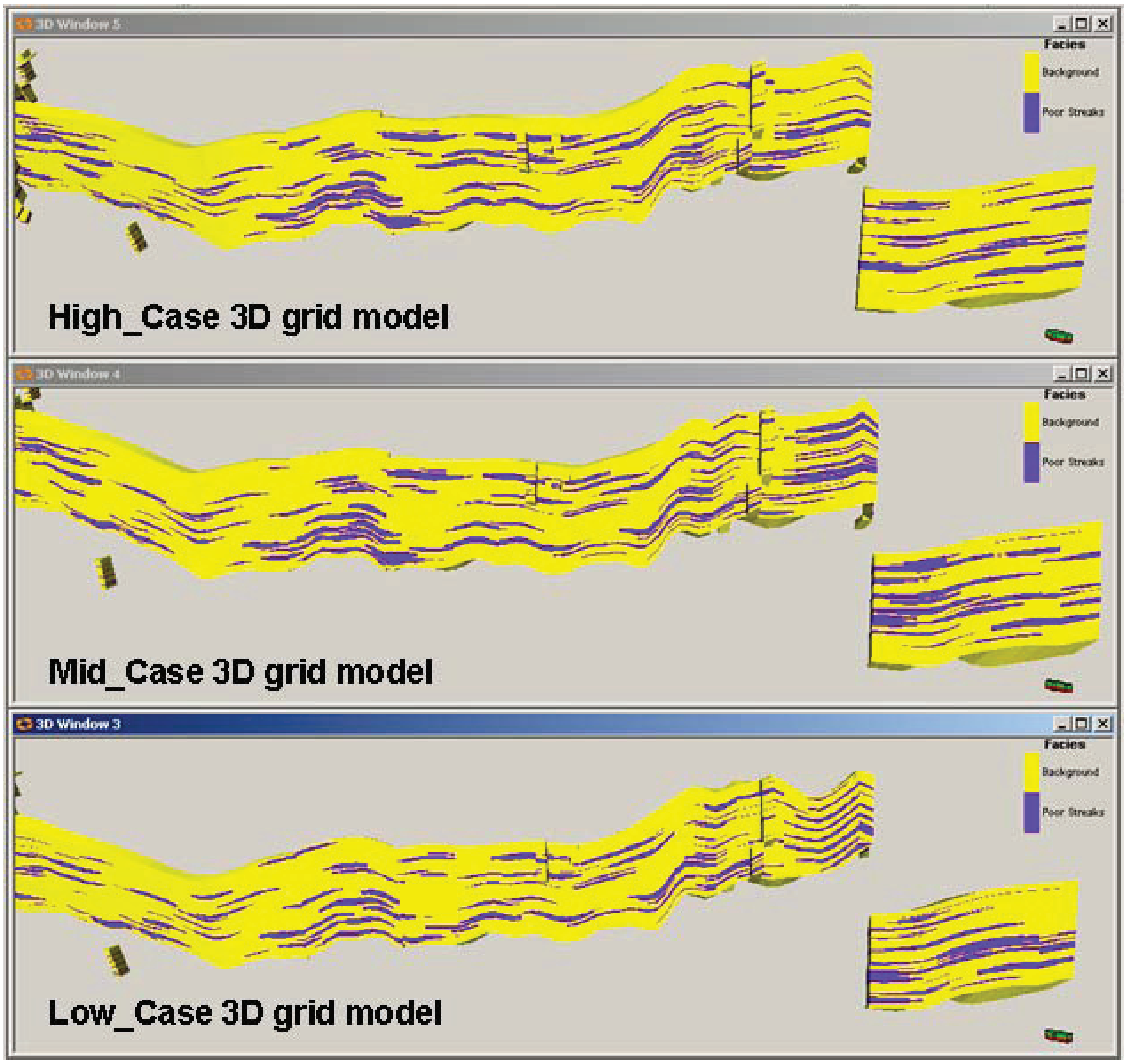

Figure 4-28 **Difference scenarios of High, Mid and Low case 3D grid model versus mid facies scenario model**

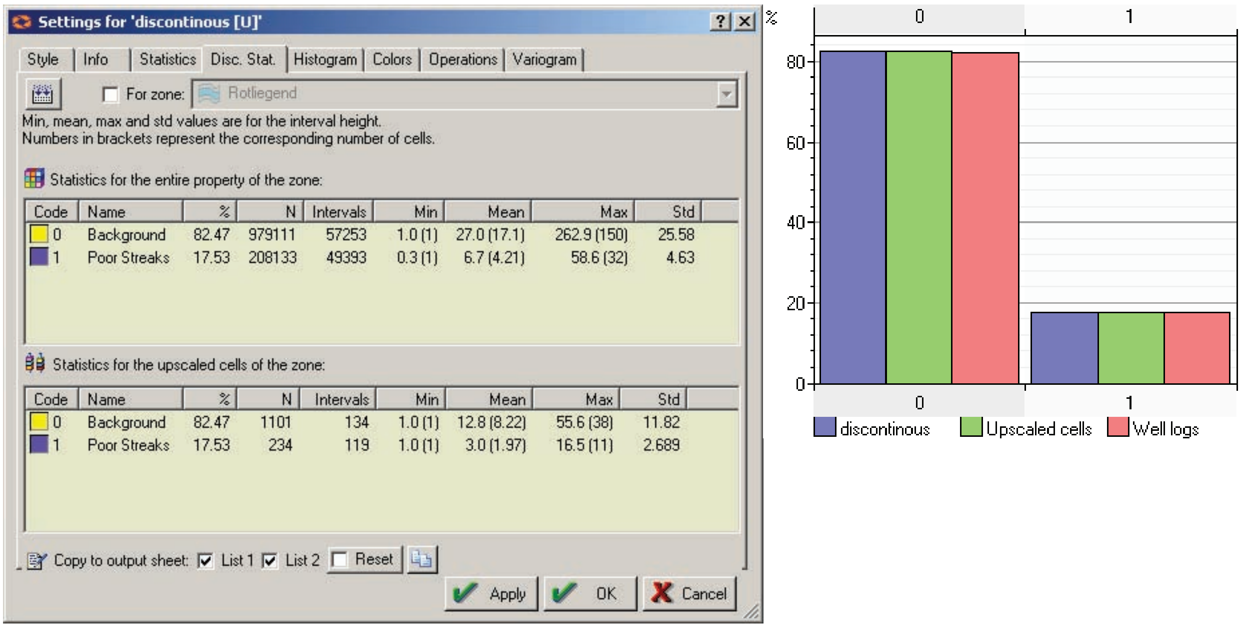

Figure 4-29 Statistics and histograms block from the discontinuous facies

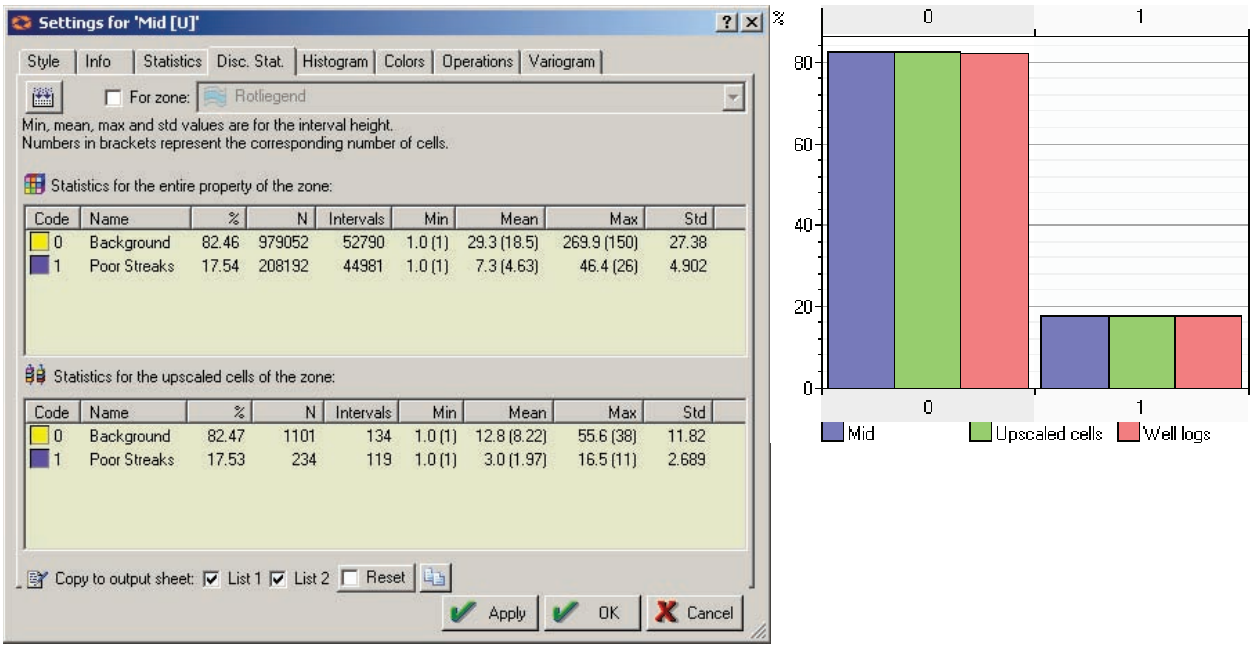

Figure 4-30 Statistics and histograms block from the mid facies

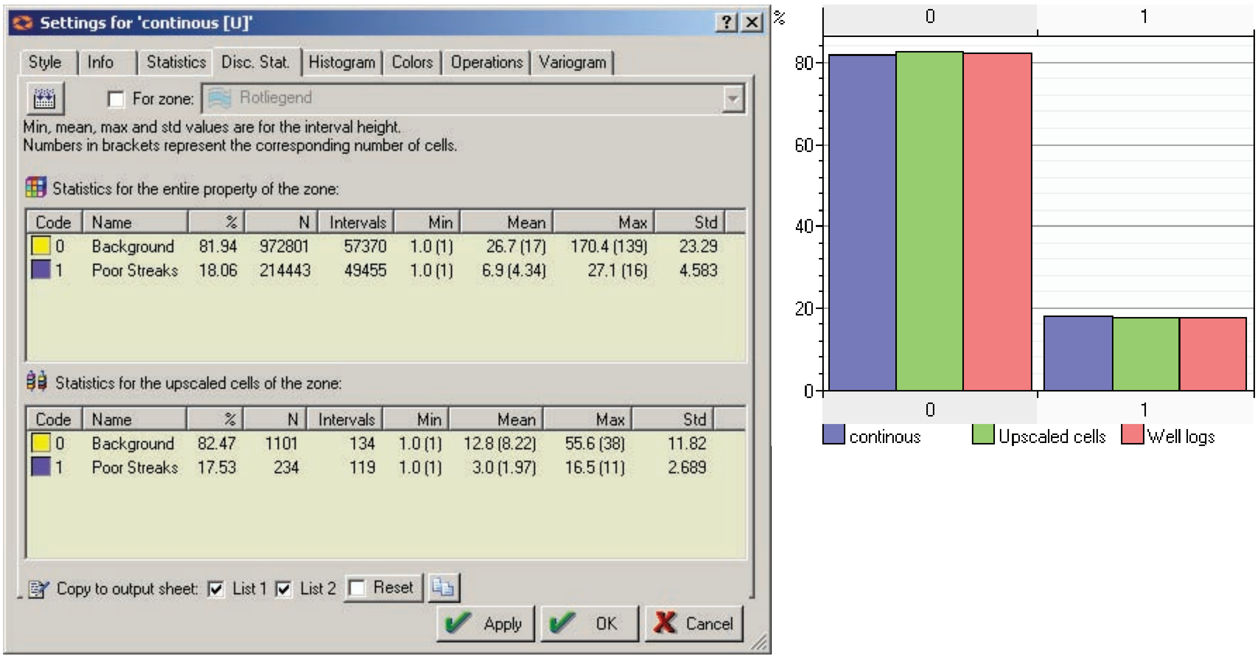

Figure 4-31 **Statistics and histograms block from the continuous facies**

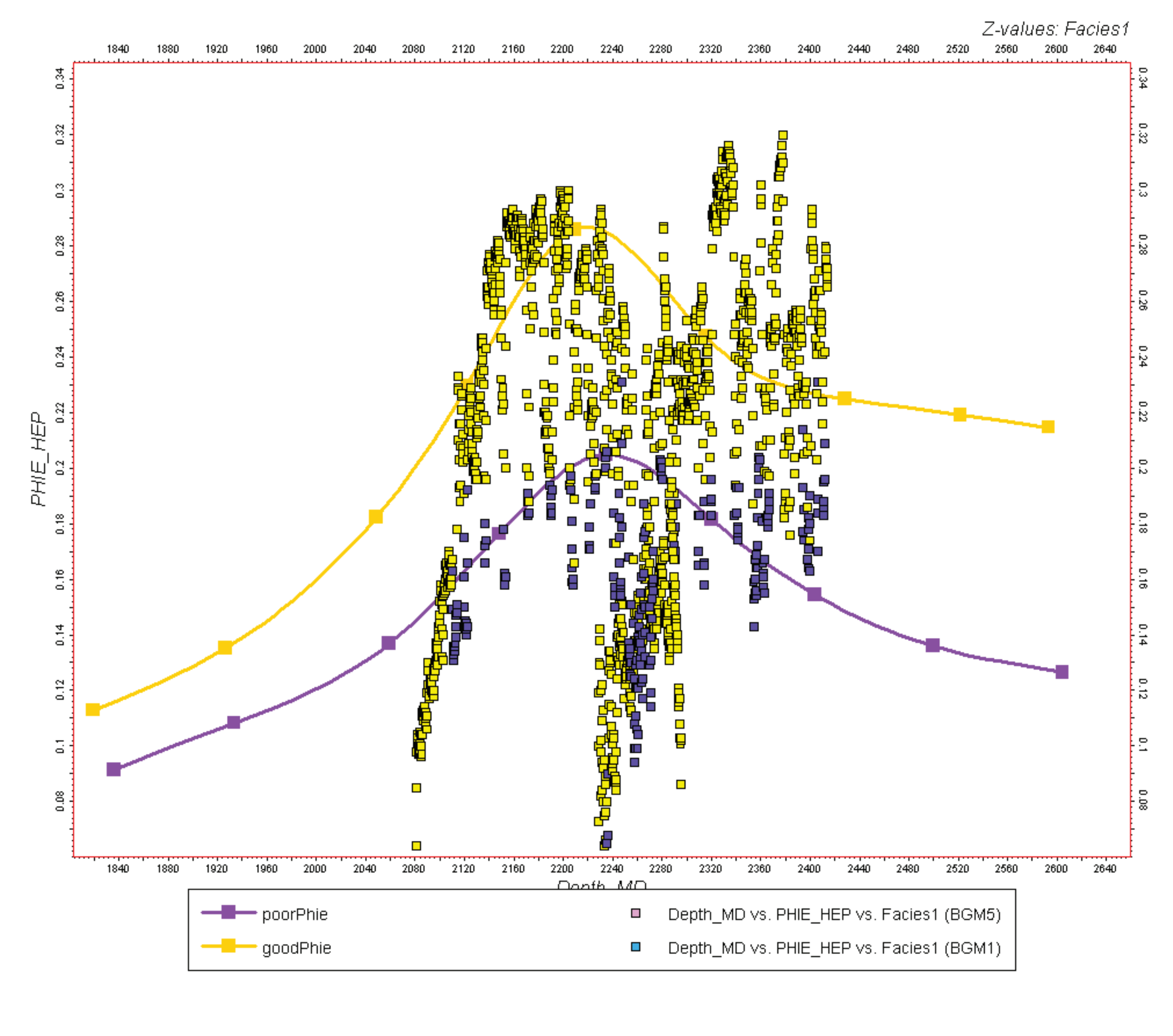

Figure 4-32 **The bell-shape curve of the good porosity (yellow line) and the low porosity streaks (purple).**

The bell-shape curve creating from BGM1 and BGM5 wells to populate the reservoir zone for Bergermeer, Groet and Bergen Fields. The curve lines are extended based on the well penetration depth in the reservoir section.

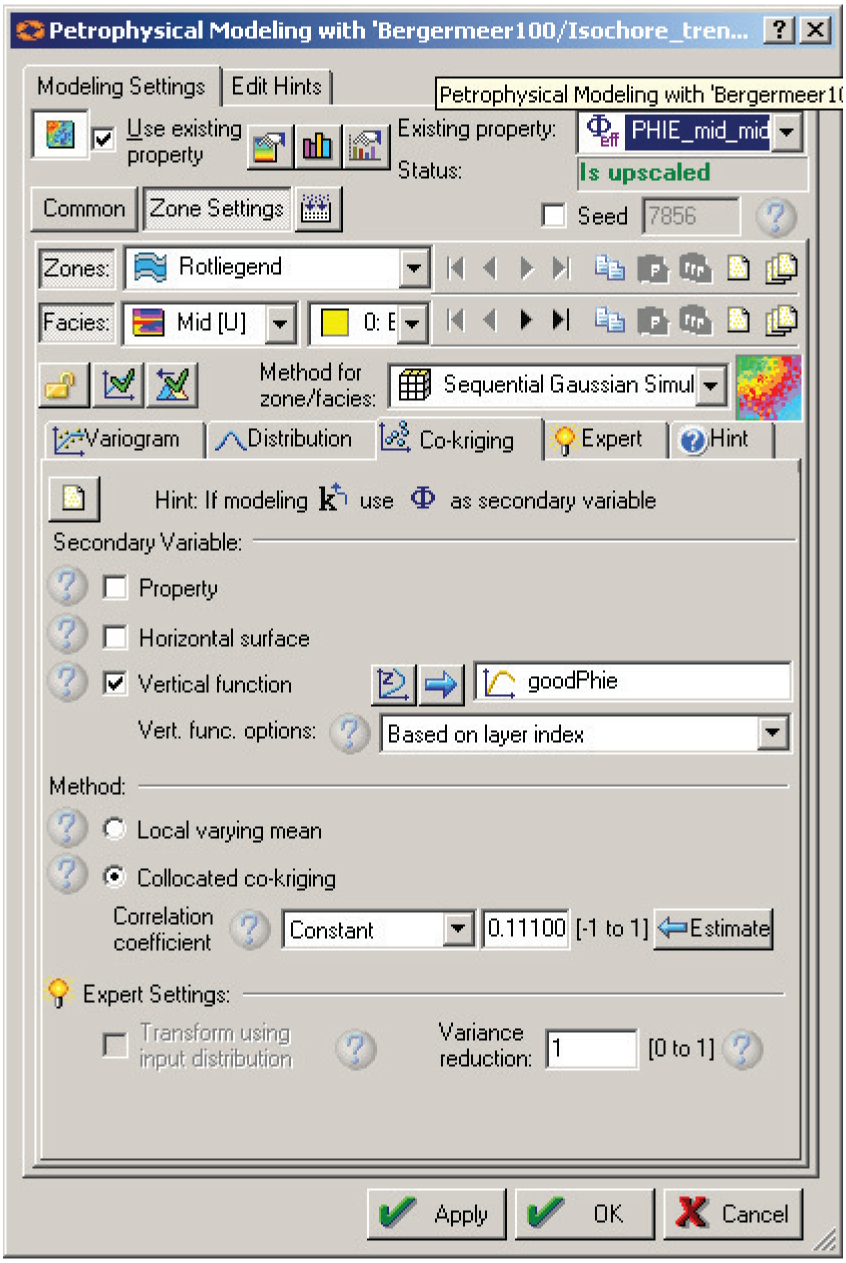

Figure 4-33 **Co-kriging settings for the application of the 'bell' curve (Figure 4-32).**

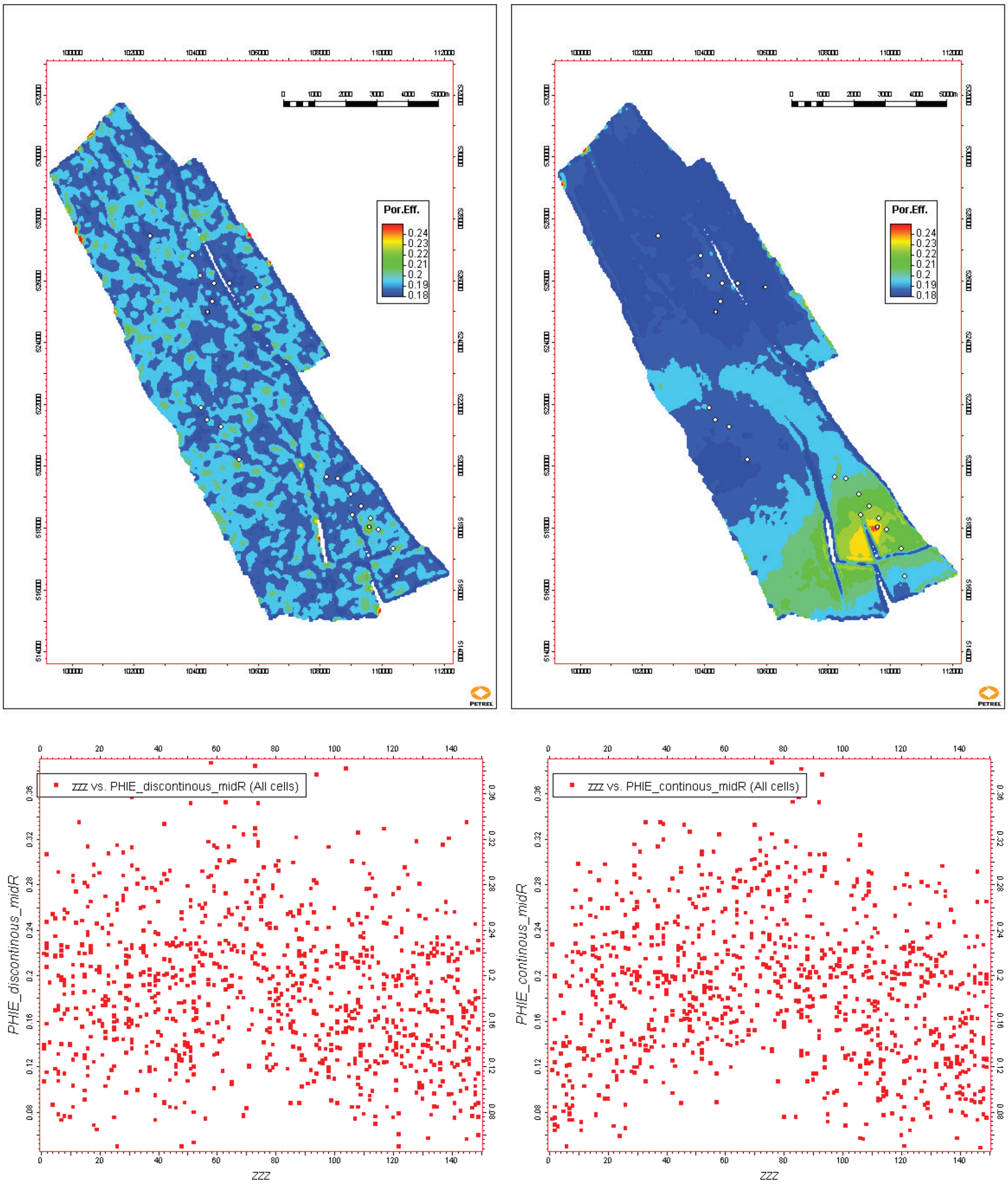

Figure 4-34 **Areal and vertical trend expressions in two scenarios. Left is 'discont_mid', right is 'cont_mid'. The top plot shows an average porosity map, the bottom a crossplot of porosity vs. K (z layer index). The 'cont_mid' scenario shows a BGM→GRT trend, as well as a quite visible 'bell' shape vertically, the former scenario does not.**

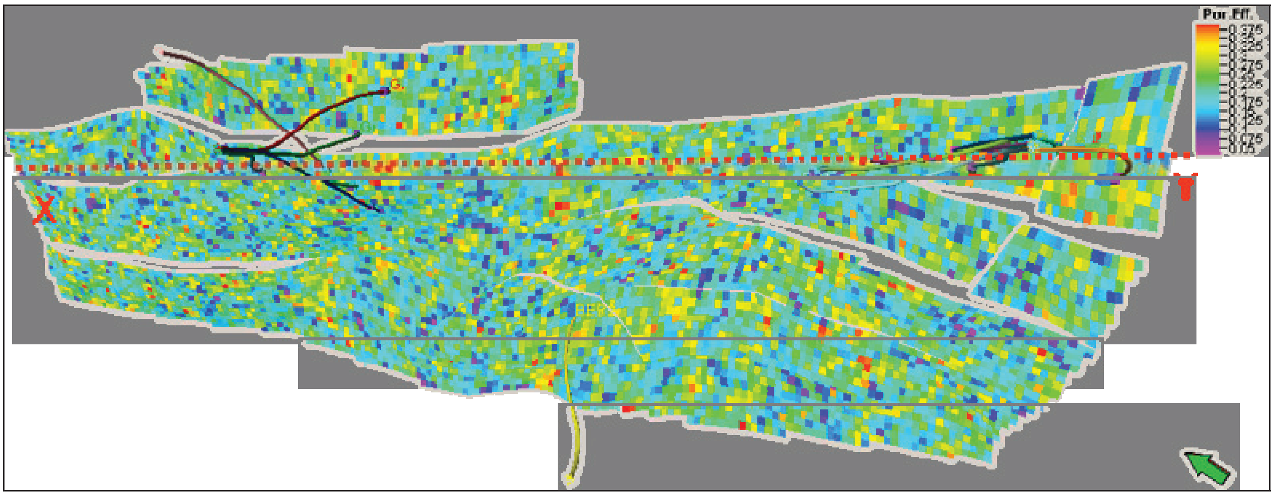

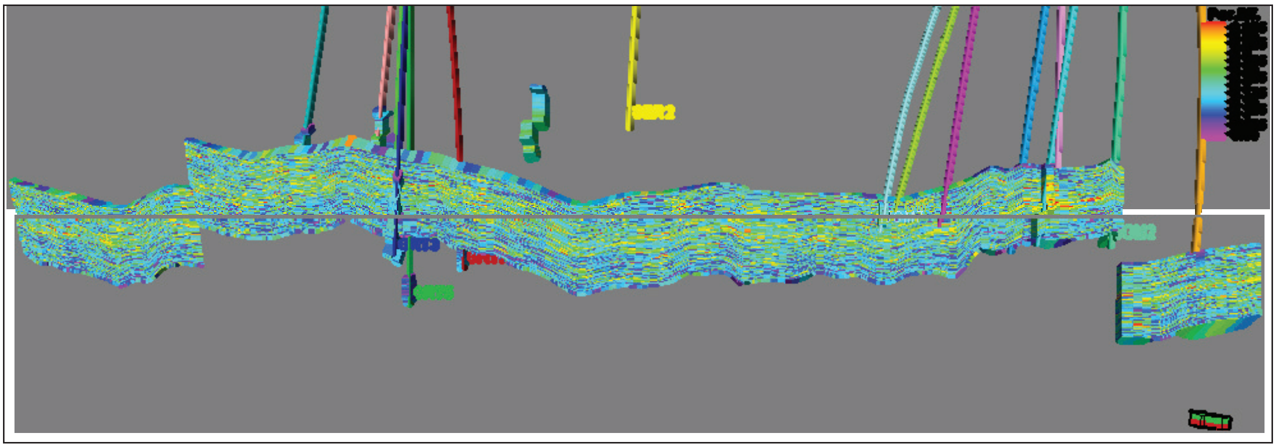

Figure 4-35 **First approach: discontinuous facies scenario VS mid lateral range, base case (3D grid without uncertainty map).**
K-layer=79 (up) and I-layer=39 (below). For facies and lateral range refer to Table 4-8, Table 4-9.

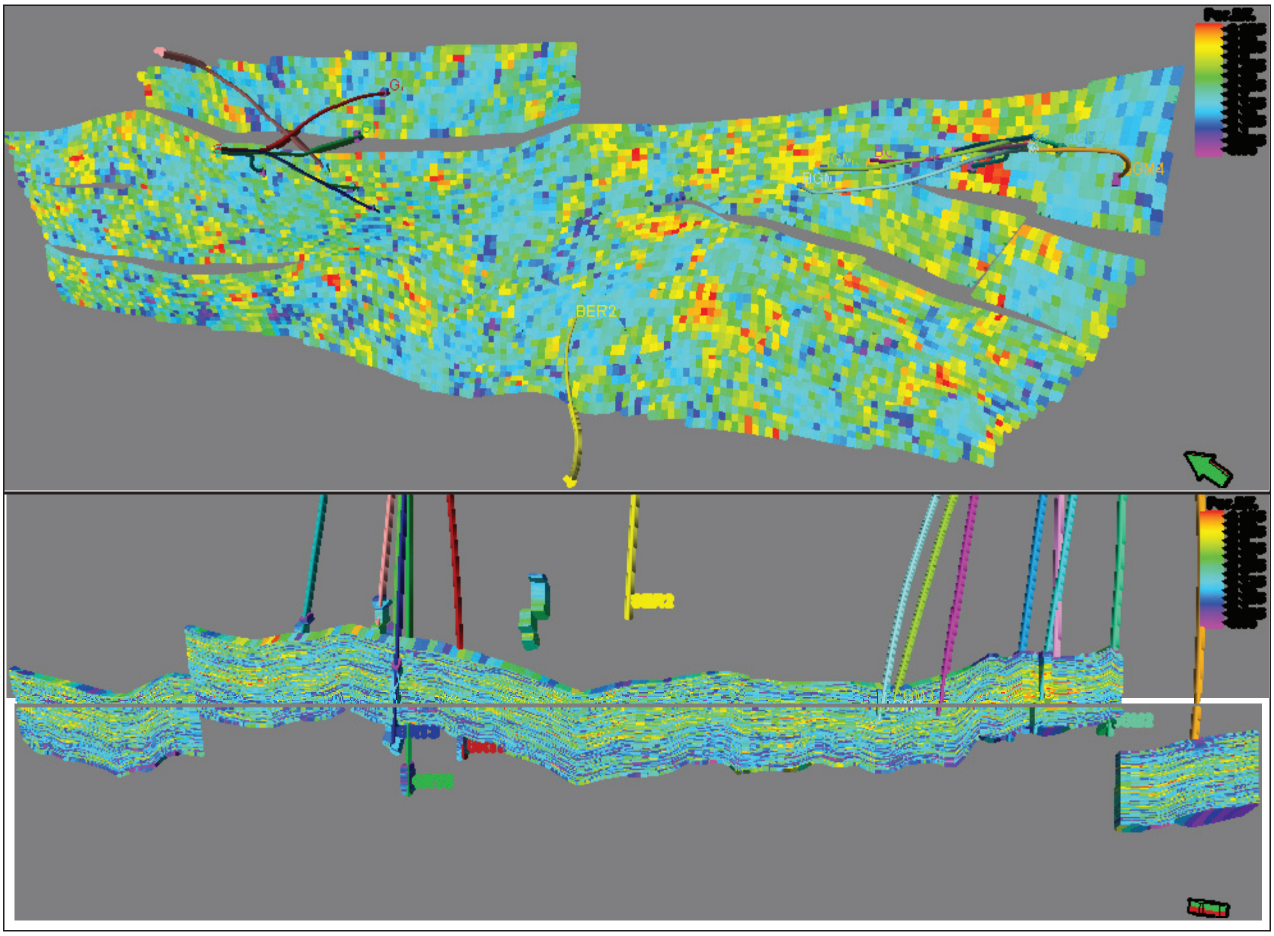

Figure 4-36 **Second approach: mid facies scenario VS low lateral range, base case (3D grid without uncertainty map)**
K-layer=79 (up) and I-layer=39 (below). For facies and lateral range refer to Table 4-8, Table 4-9.

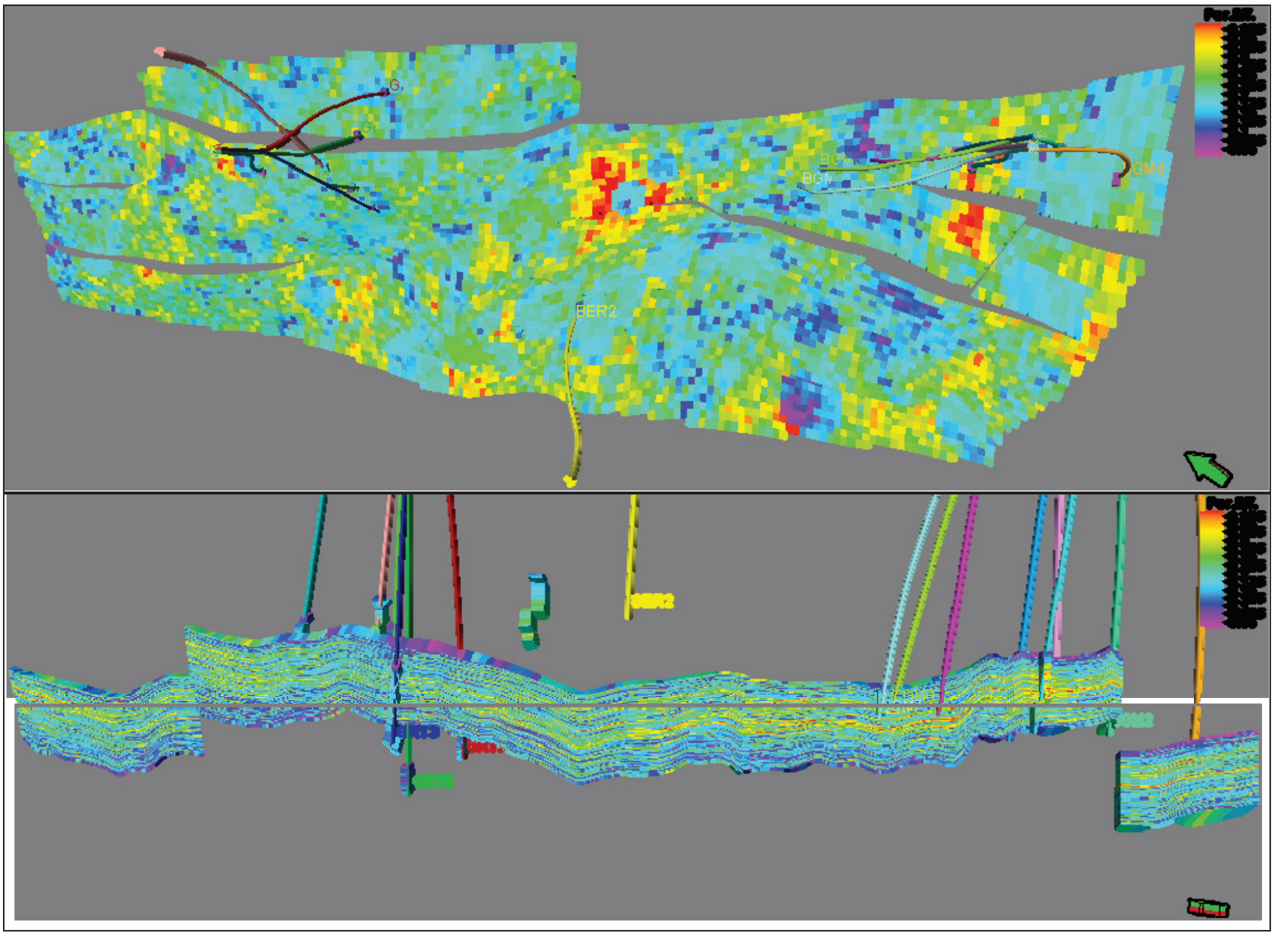

Figure 4-37 **Third approach: mid facies scenario VS mid lateral range, base case (3D grid without uncertainty map)**
K-layer=79 (up) and I-layer=39 (below). For facies and lateral range refer to Table 4-8, Table 4-9.

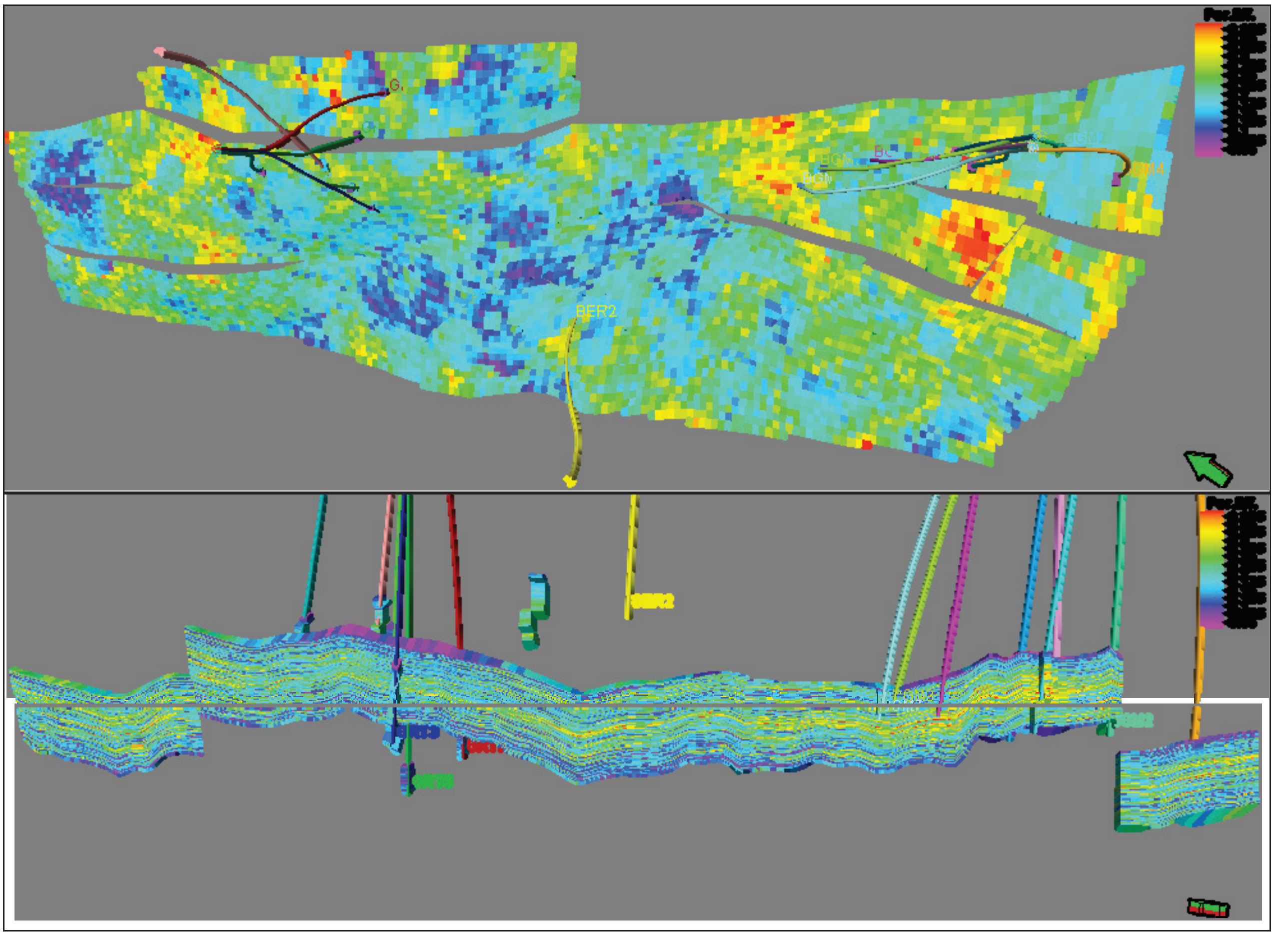

Figure 4-38 Fourth approach: mid facies scenario VS high lateral range, base case (3D grid without uncertainty map)
K-layer=79 (up) and I-layer=39 (below). For facies and lateral range refer to Table 4-8, Table 4-9.

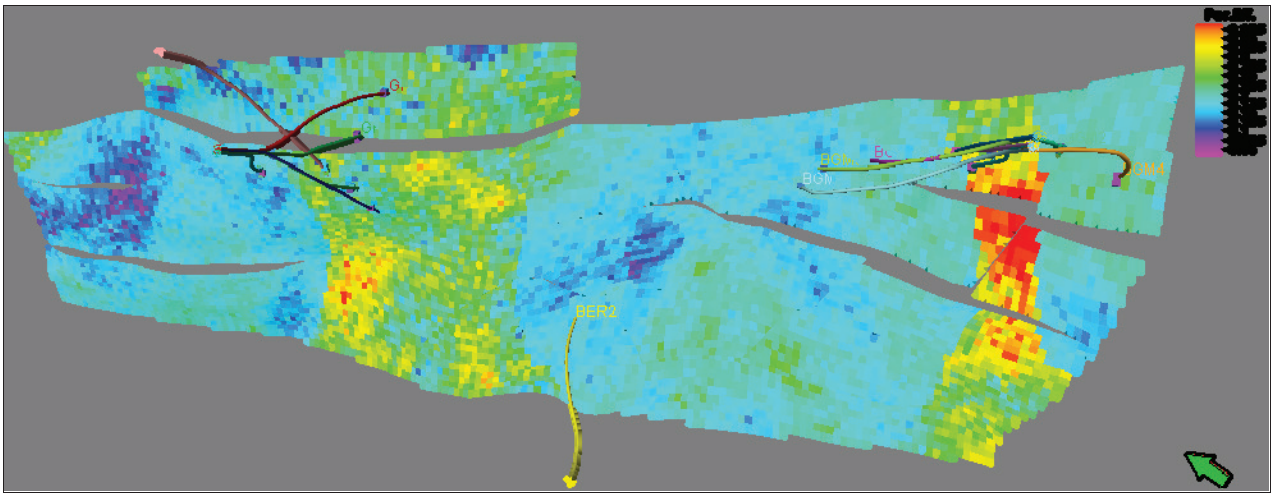

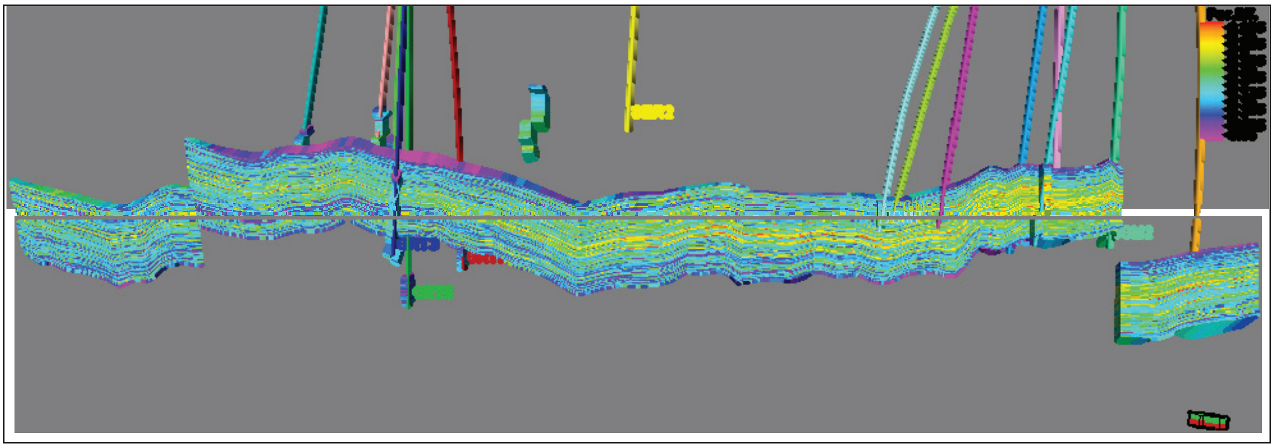

Figure 4-39 **Fifth approach: continuous facies scenario VS mid lateral range, base case (3D grid without uncertainty map)**
K-layer=79 (up) and I-layer=39 (below). For facies and lateral range refer to Table 4-8, Table 4-9.

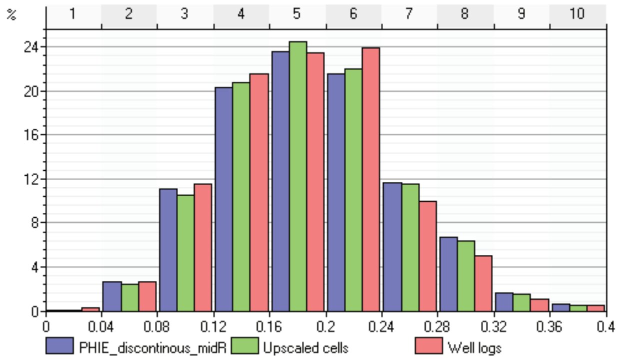

Histogram for PHIE_discontinues_midR

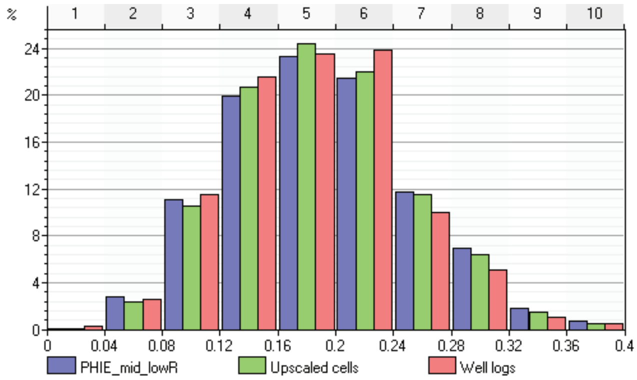

Histogram for PHIE_mid_lowR

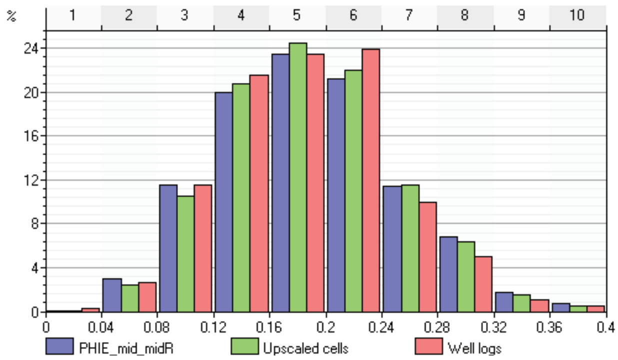

Histogram for PHIE_mid_midR

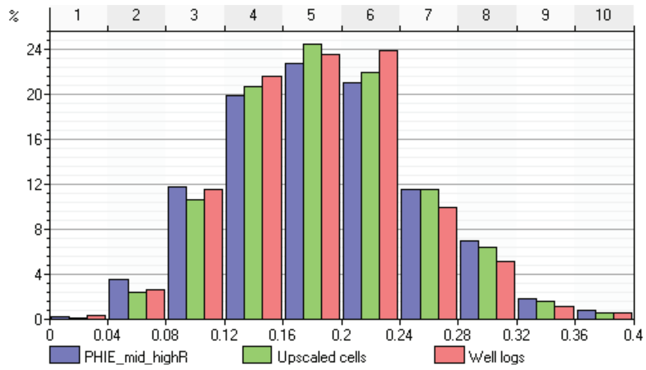

Histogram for PHIE_mid_highR

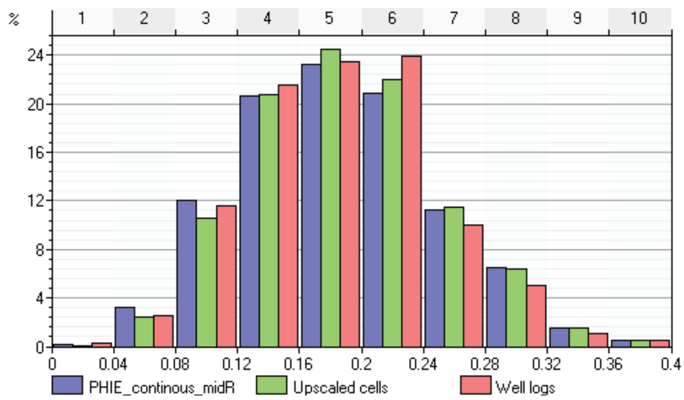

Histogram for PHIE_continues_midR

Figure 4-40 **Histograms block for different porosity modelling approach comparing porosity calculated (blue), upscalled porosity (green) and porosity well logs (red)**

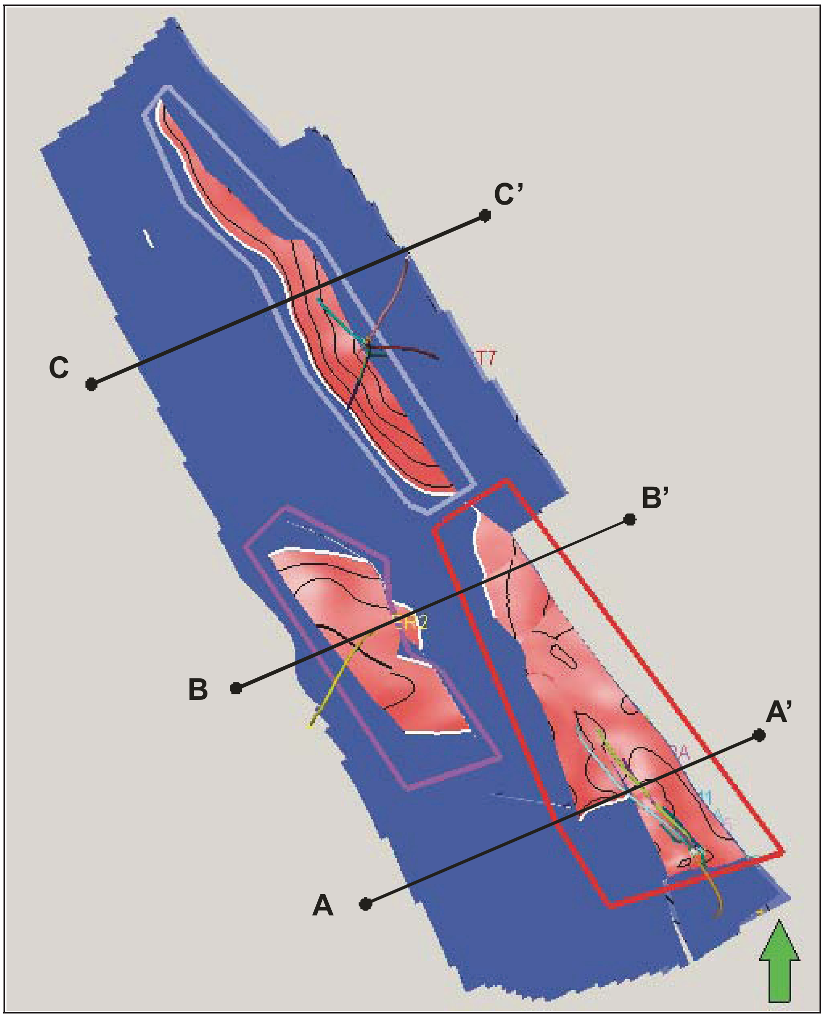

Figure 4-41 The GWC (blue) and the fluid polygons in the modelling area

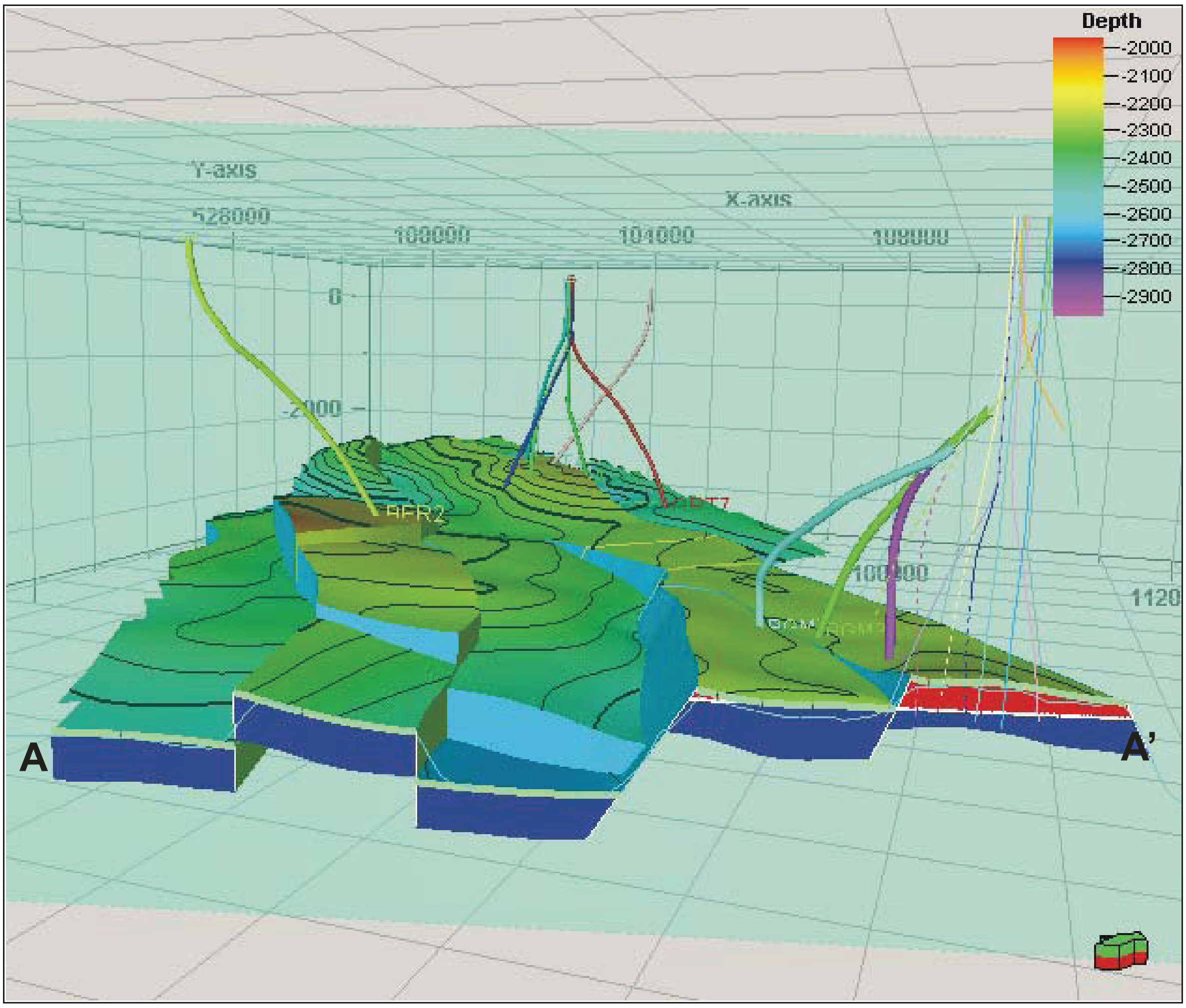

Figure 4-42 **A-A' cross section of Bergermeer Field showing the GWC contacts**
The green line is Top ROSLU horizon that created from make horizon process. The light blue line is an input data from Top ROSLU surface.

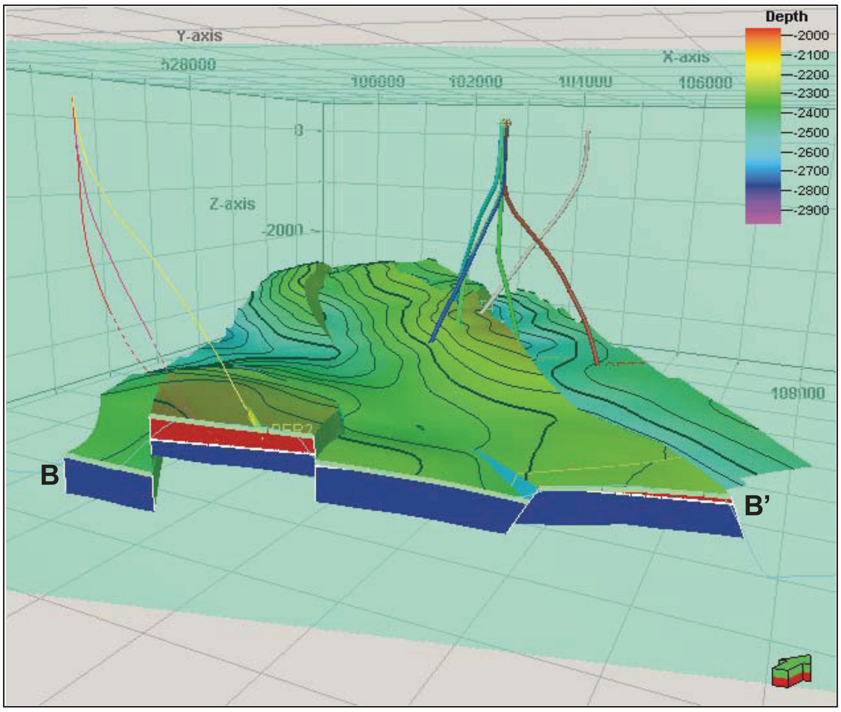

Figure 4-43 B-B'cross section of Bergen Field showing the GWC contacts

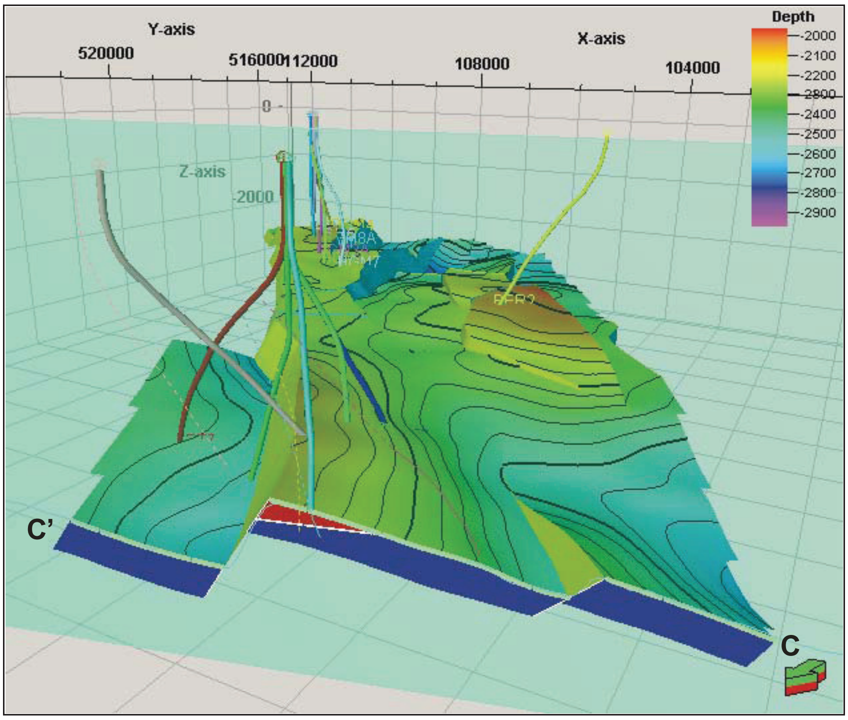

Figure 4-44 C-C' cross section of Groet Field showing the GWC contacts
The cross-section is looking at south.

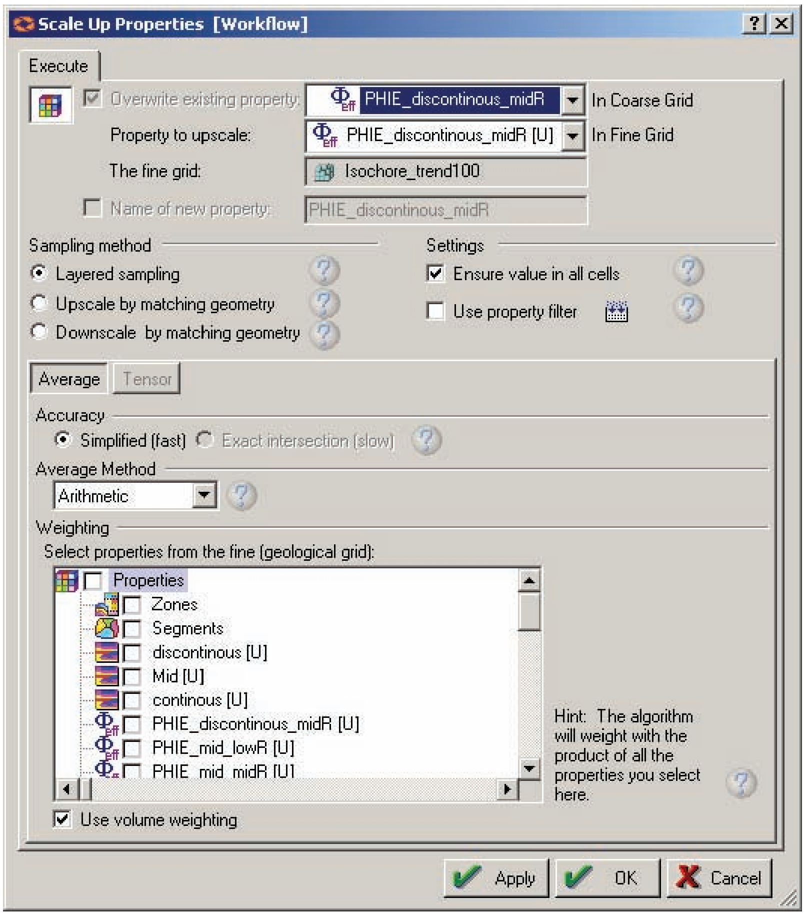

Figure 4-45 Settings for upscaling porosity from static model grid to flow simulation grid.

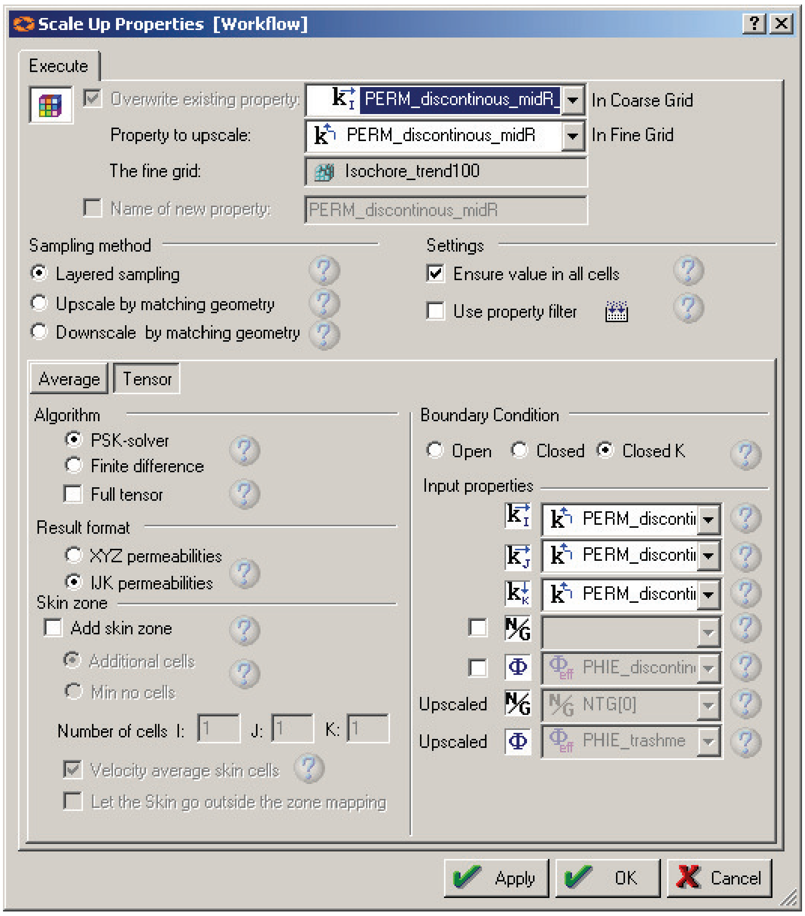

Figure 4-46 **Settings for upscaling permeability from static model grid to flow simulation grid. The label 'tensor' does not imply that the resulting permeability is actually a tensor; it signifies that the actual distribution of the static model cell permeabilities within the flow simulation cell is taken into account; vertical permeability will turn our lower than horizontal permeability 'automatically' (Figure 4-47).**

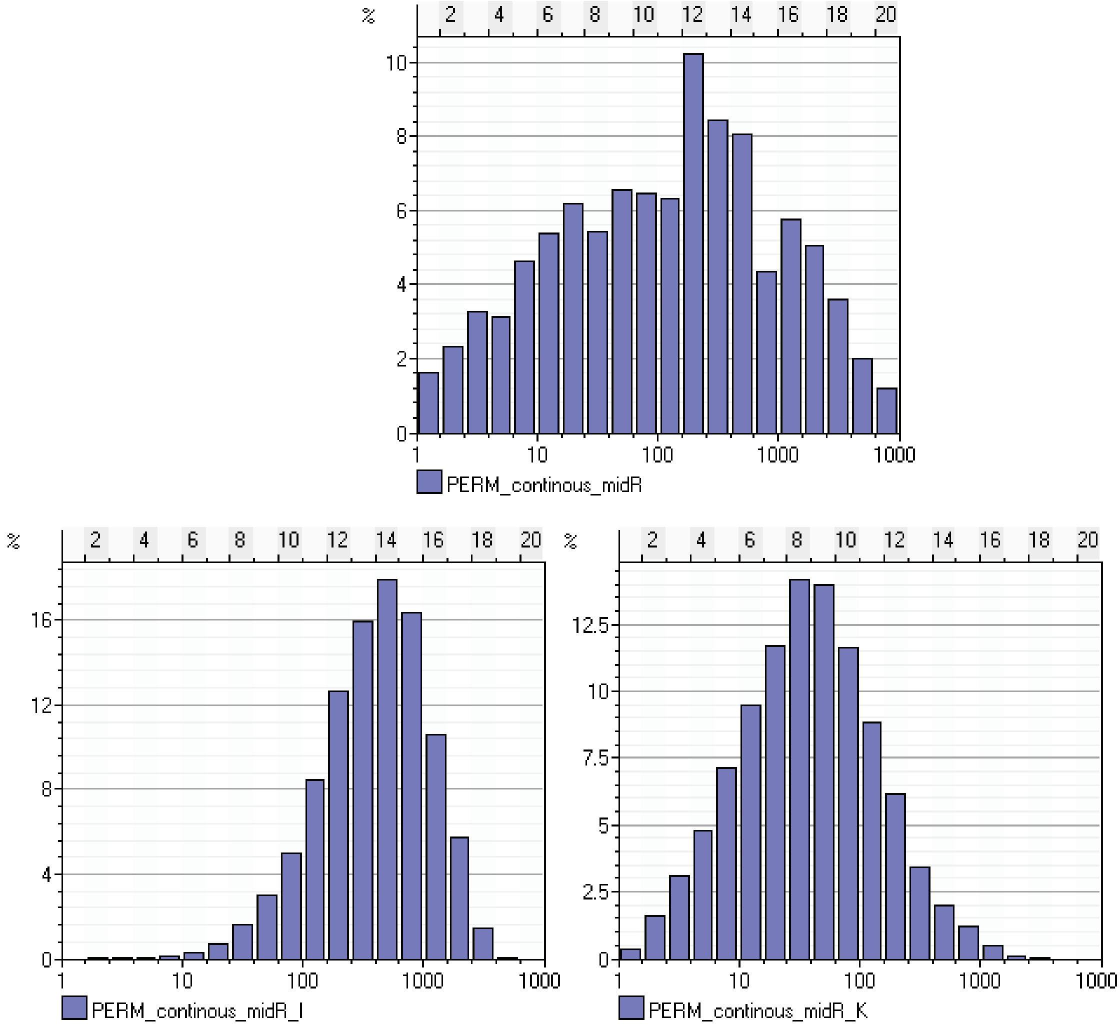

Figure 4-47 **Permeability histogram before upscaling (top), and after upscaling (bottom left: k_x; bottom right: k_z). The difference between horizontal and vertical permeability is a result of upscaling alone, not of any explicit multiplier. (The case displayed is the 'continuous mid' [Table 4-8] case.)**

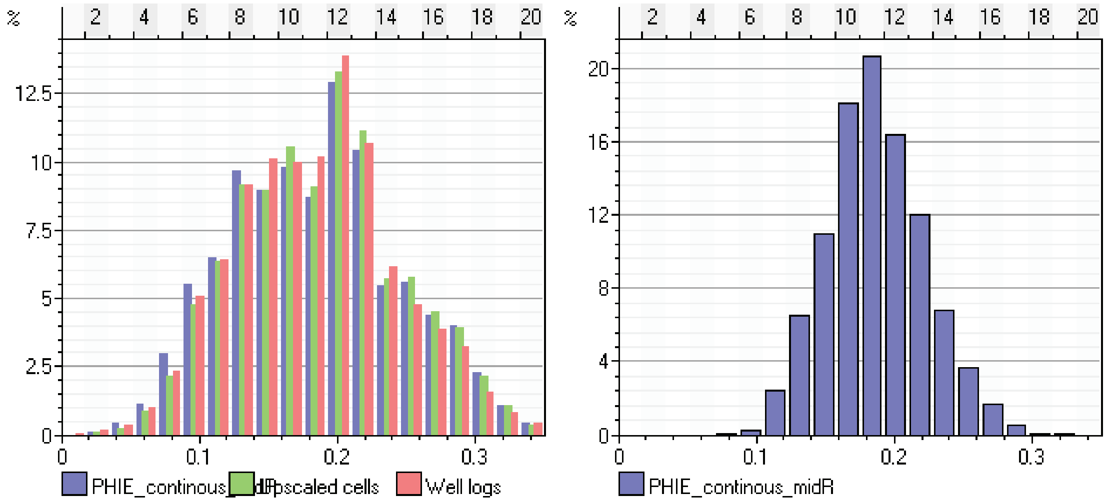

Figure 4-48 **Porosity histogram before upscaling (left), and after upscaling (right). (The case displayed is the 'continuous mid' [Table 4-8] case.)**

References

[1] *Petrophysical Evaluation of the Bunter, Zechstein and Rotliegende Formations; Onshore Bergen Concession, Netherlands*; I Stockden, BP; October 2004

[2] *BERGERMEER NO.1 (BUNTER SANDSTONE AND ROTLIEGENDES) CORE ANALYSIS RESULTS*; 1969(?), Received from Taqa.

[3] *Log Interpretation Principles/Applications*, Schlumberger, 1989

[4] *Theory, Measurement, and Interpretation of Well Logs*, Z. Bassiouni, SPE, 1994

[5] *Chart Book*, Schlumberger, 1989

[6] *Rock Physics Handbook*, Mavko, Mukerji and Dvorkin, Cambridge University Press, 1998

[7] Geluk M. (2005) Permian and Triassic basins in the Netherlands: Stratigrapy, Tectonics and paleogeography. In Geluk M. (ed) Stratigraphy and Tectonics of Permo-Triassic Basins in the Netherlands and Surrounding Areas. Nederlandse Aardolie Maatschapppij (NAM) B.V. Ch.4: p. 61-72.

[8] Glennie K.W. (1998) Lower Permian – Rotliegend. In Glennie K.W. (ed) Introduction to the Petroleum Geology of the North sea. 4th edition, Blackwell Scient. Publ., Oxford, p. 137-173.

[9] Slatt R.M. (2006) Eolian (windblow) deposits & reservoir. In Slatt R.M. (ed) Stratigraphic Reservoir Characterization for Petroleum Geologists, Geophysicists and Engineers. Elsevier B.V. Ch 7: p. 249-274.

[10] Tobin R.C., Petrographic Evaluation of Rotliegendes Reservoir Sandstones, Amoco #1 Bergermeer, Onshore Netherlands

[11] “Operational Lithostratigraphy of the Netherlands”, version 1.1, NAM Assen Exploration

[12] “Fundamentals of gas reservoir engineering” by J. Hagoort, Elsevier, page 34.

[13] Hall, KR and Yarborough L, “A new equation of state for z-factor calculations”, Gas technology, SPE reprint series no 13, vol 1, 1977.

[14] Thodos Algorithm

[15] Special Core Analysis Study; Bergermeer No. 1 and 2 Wells; Core Labs; 1971 [SCAL 70187]

[16] *GWC rise Bergermeer field*; Note, Taqa

[17] *Feasibility of peak shaving using concession gas reservoirs*; Hagoort & Associates BV, January 1994

[18] *Feasibility of gas storage in the Bergermeer reservoir*; Hagoort & Associates BV, May 1988

[19] Expro Operation report – Amoco Netherlands Petroleum Company, Bergermeer 1, BHP and BHT surveys during well test, 4th April – 7th April 1979.

Appendix I.A Petrographic Evaluation Summary

Remarks: The Petrographic evaluations were provided by Taqa [10], but the core descriptions were done in TNO core shed, Utrect dated 14 March 2007.

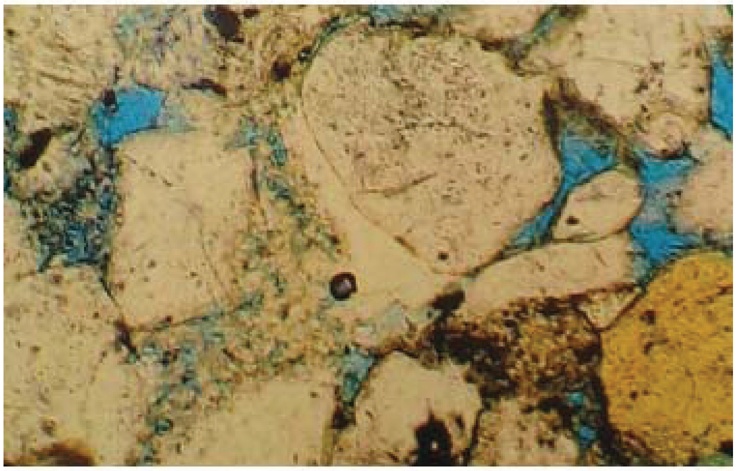

Left: The core is characterized by non horizontal lamination sandstone, porous, well sorted sandstone laminated with hematite.

Up-right: Sandstone, typically representative of Quartz and dolomite cemented lithofacies rocks from this reservoir. The patchy distribution of macroporosity (blue) and the moderately compacted nature of the detrital framework.

Lower-right: A well developed rim of syntaxial quartz overgrowth cement (center) flanked by a pore-filling cluster of Kaolinite marix (greenish). 200x uncrossed nicol.

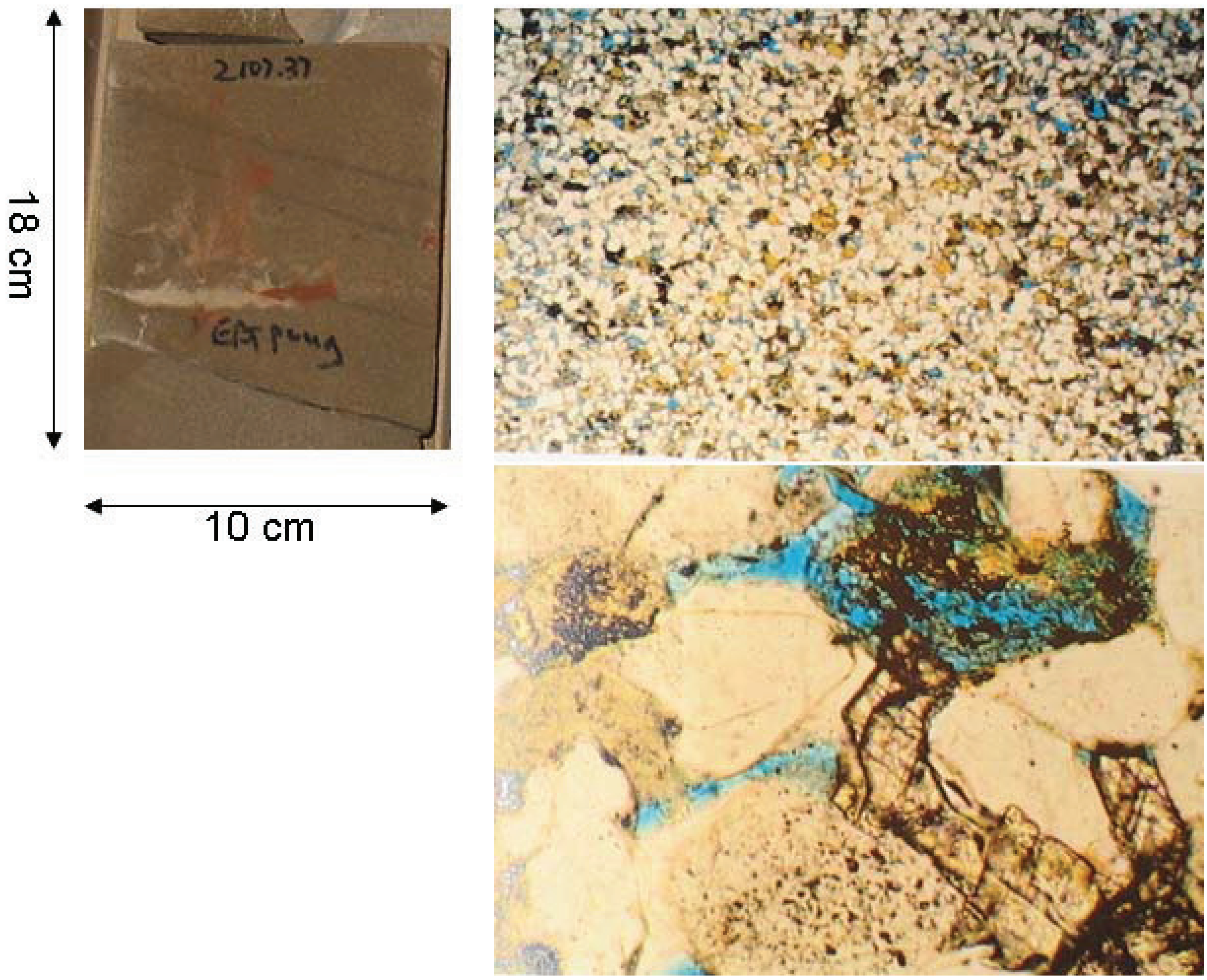

Left: The core in BGM1 at 2107.37 m is characterized by non non-horizontal sandstone bed laminated with hematite, porous, medium well-sorted sandstone and anhydrite healed fracture occurrence crossing the bedding.

Up-right: a low magnification view of this quartz and dolomite cemented lithic arkosic sandstone from the upper tight zone of the reservoir. 16x uncrossed nicol.

Lower-right: Pore-filling dolomite cement (lower-right) post-dating quartz overgrowth cement (center). 200x uncrossed nicols.

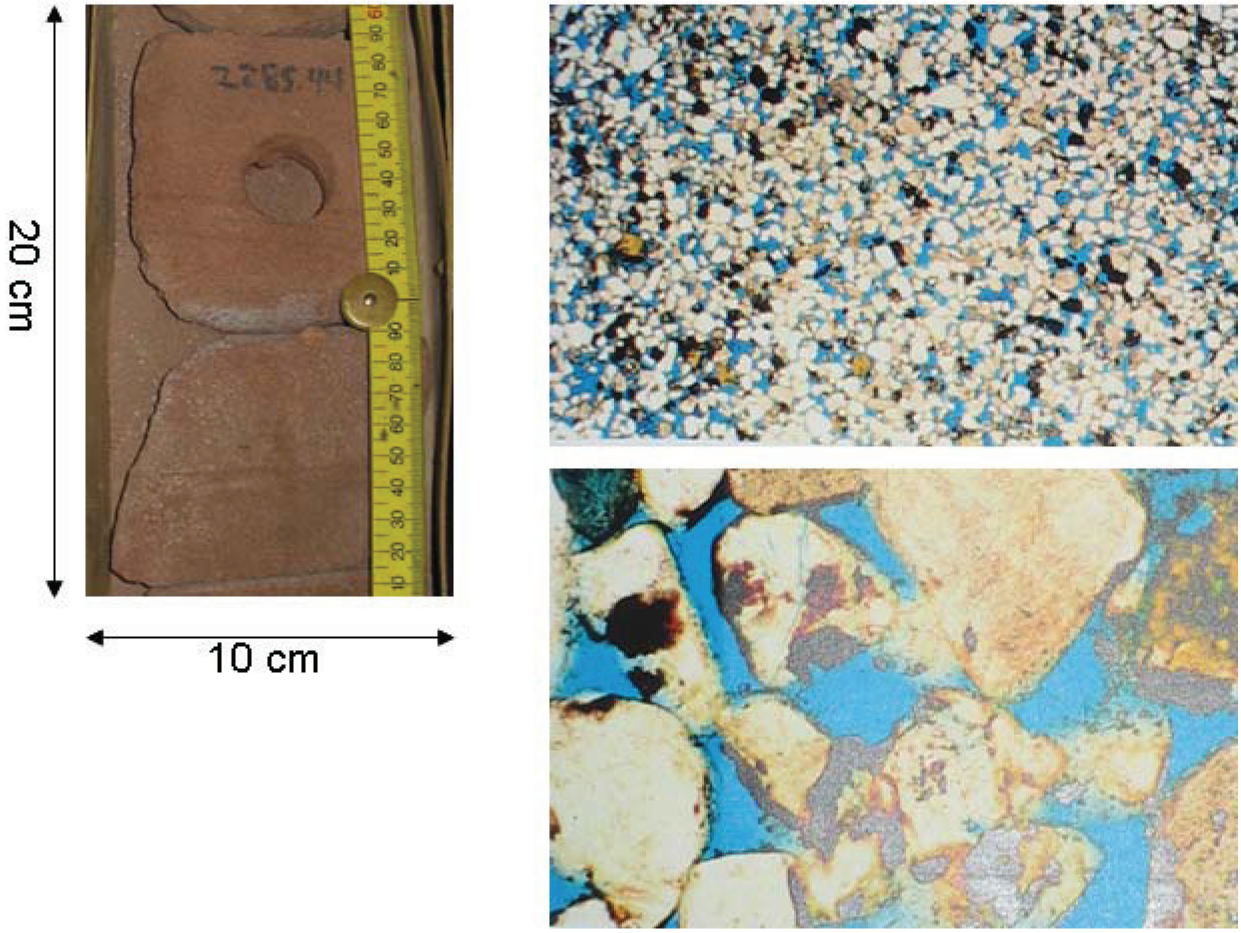

Left: The core in BGM1 at 2285.43 m interpreted as sand flat facies which is characterized by non-horizontal lamination sandstone, porous, medium well-sorted sandstone laminated with thin layer of hematite and spotty anhydrite occurrence.

Up-right: A low magnification view of porous, slightly cemented feldspathic litharnitic sandstone from the lower porous zone of the reservoir. 16x uncrossed nicols.

Lower-right: Hematite cement occurs as a widespread grain coating cement within this sandstone. Note the mildly compacted detrital grains in this field of view. 200x uncrossed nicol.

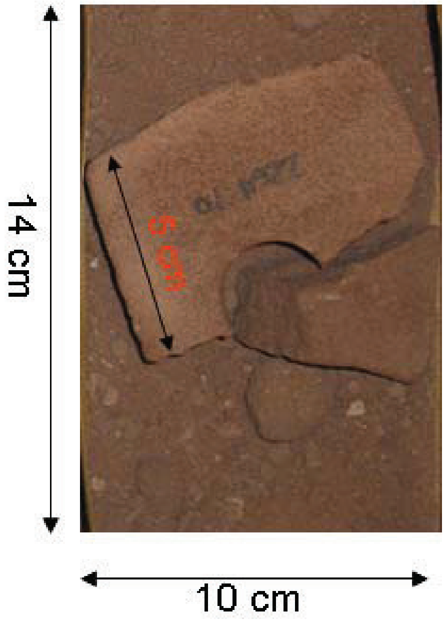

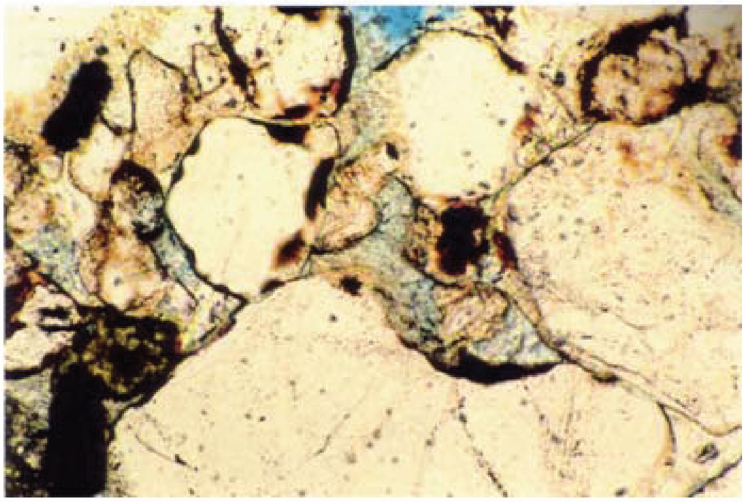

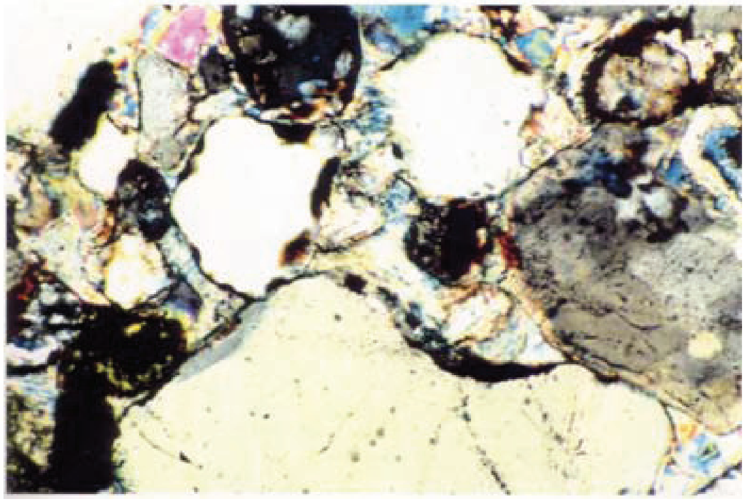

Left: The core in BGM1 at 2264.69 m interpreted as sand flat facies which is characterized by regular lamination sandstone, porous, medium well-sorted sandstone and spotty anhydrite occurrence.

Up-right: A patch of pore-filling gypsum cement that has been leached to yield traces of interparticle dissolution porosity (blue-green: center). 200x uncrossed nicols.

Lower-right: As figure above, with 200x crossed nicols. Note the marginally hydrated character of the andhydrite cement along the upper margin or this photo.

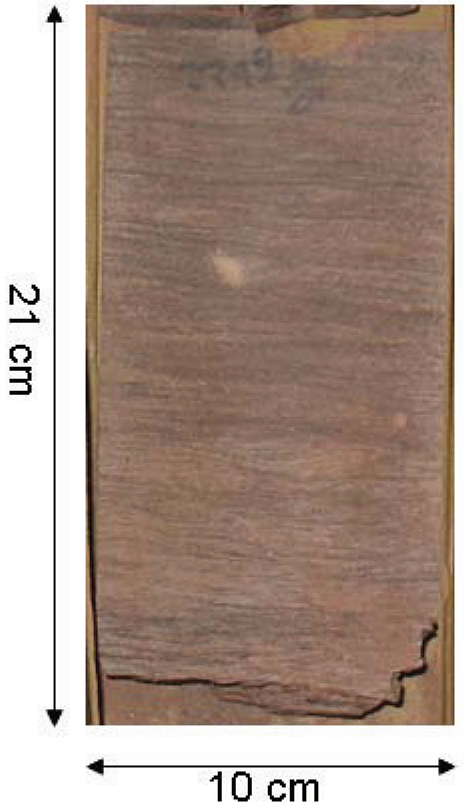

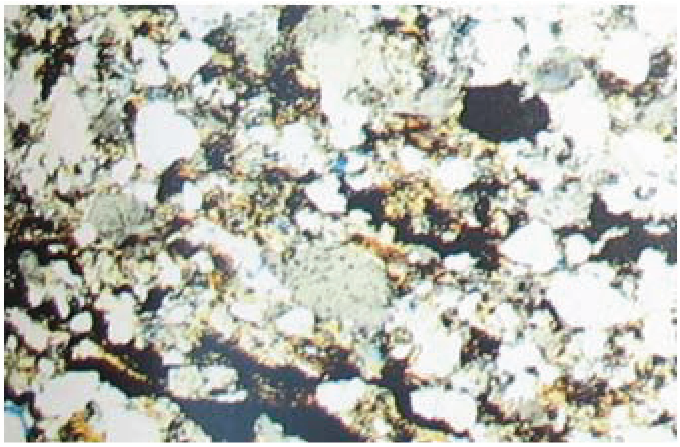

Left: The core in BGM1 at 2298.21 m interpreted as sand flat facies which is characterized by irregular wavy lamination between shale and sandstone, densely compact, less porous, fine well-sorted sandstone.

Up-right: A low magnification view of the only representative of the matrix-rich lithic arkosic sandstone lithofacies. 16x uncrossed nicol.

Lower-right: The interparticle space in this sandstone is filled with a combination of illitic clay matrix, iron oxide cement, and siderite. The thin section from this interval contains no macroporosity. 100x uncrossed nicols.

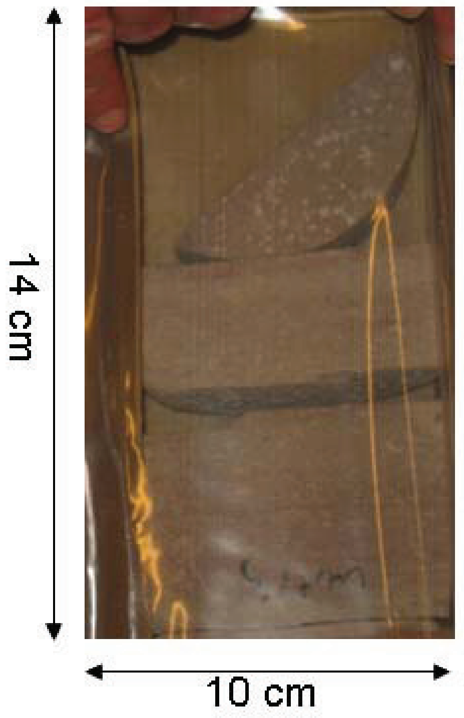

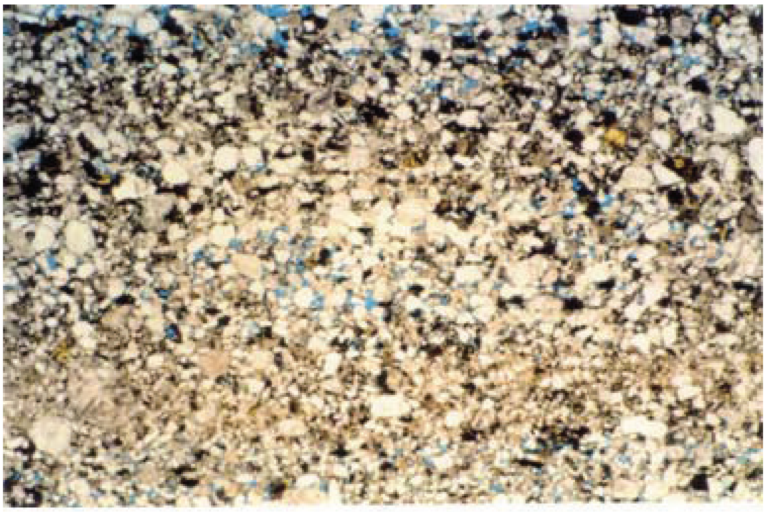

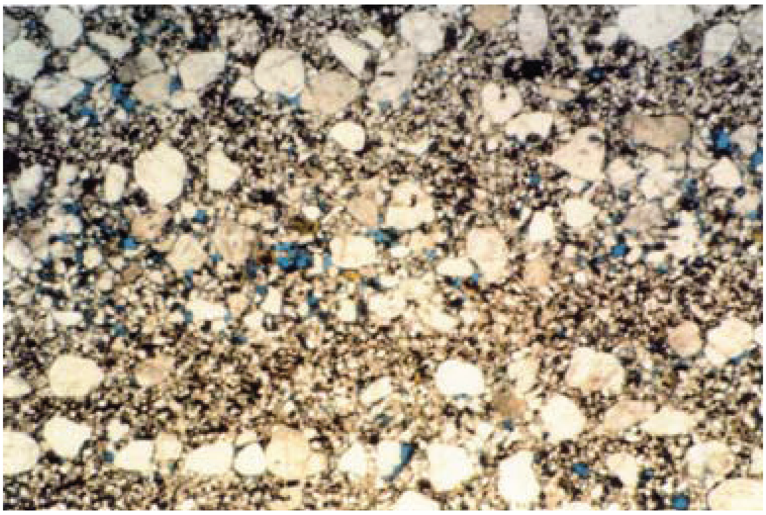

Left: The core in BGM1 at 2236.71 – 2245 m interpreted as sand flat facies which is characterized by regular lamination shale and sandstone, less porous, medium well-sorted sandstone and spotty anhydrite occurrence.

Up-right: A low magnification view of this laminated, densely compacted, relatively non porous, lithic arkosic sandstone. 16x uncrossed nicol.

Lower-right: The bulk of the macroporosity within this laminated sandstone is concentrated in the relatively coarse-grained interbeds (e.g. center). 16x uncrossed nicol.

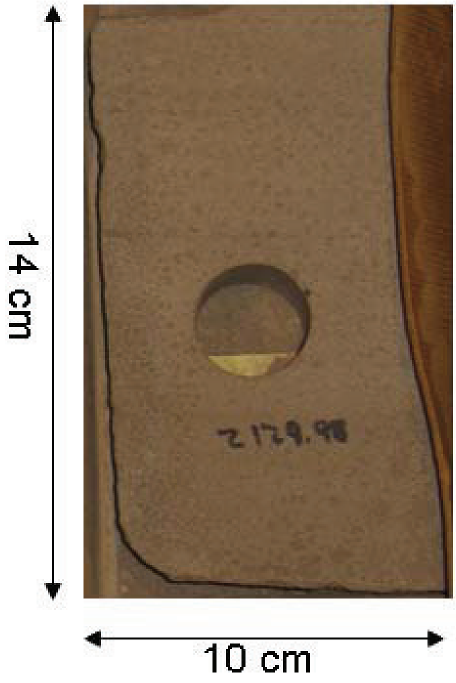

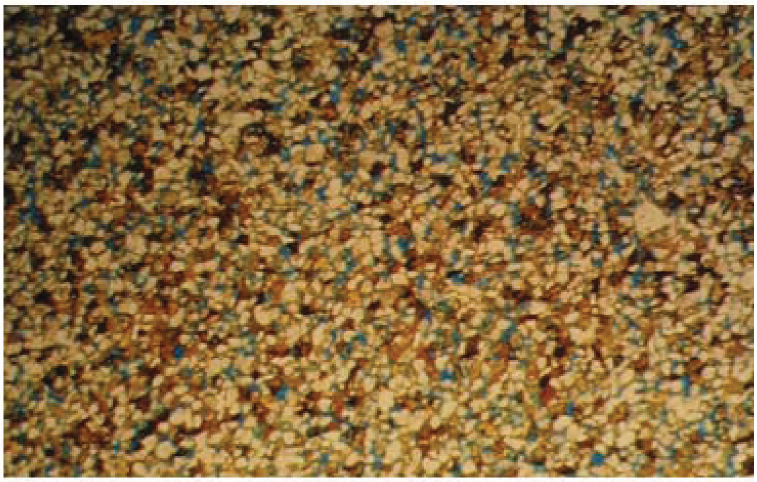

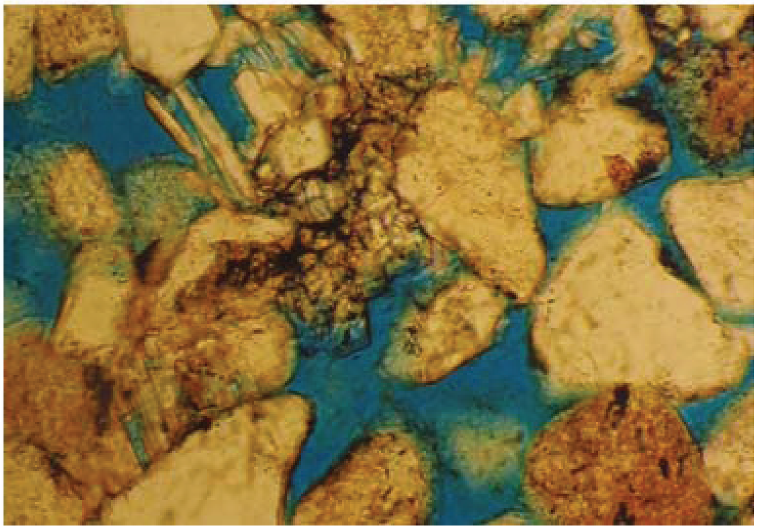

Left: The core in BGM1 at 2129.98 m interpreted as sand flat facies which is characterized by regular lamination sandstone, porous, medium well-sorted sandstone and spotty anhydrite occurrence.

Up-right: a low magnification view of this porous and permeable, slightly cemented, lithic arkosic sandstone. This sandstone is vertically positioned near the base of the upper tight zone. 16x uncrossed nicol.

Lower-right: A detailed view of a marginally corroded cluster of dolomite cement (center). Note the leached plagioclase feldspar grains in the top half of photomicrograph. 200x uncrossed nicols.

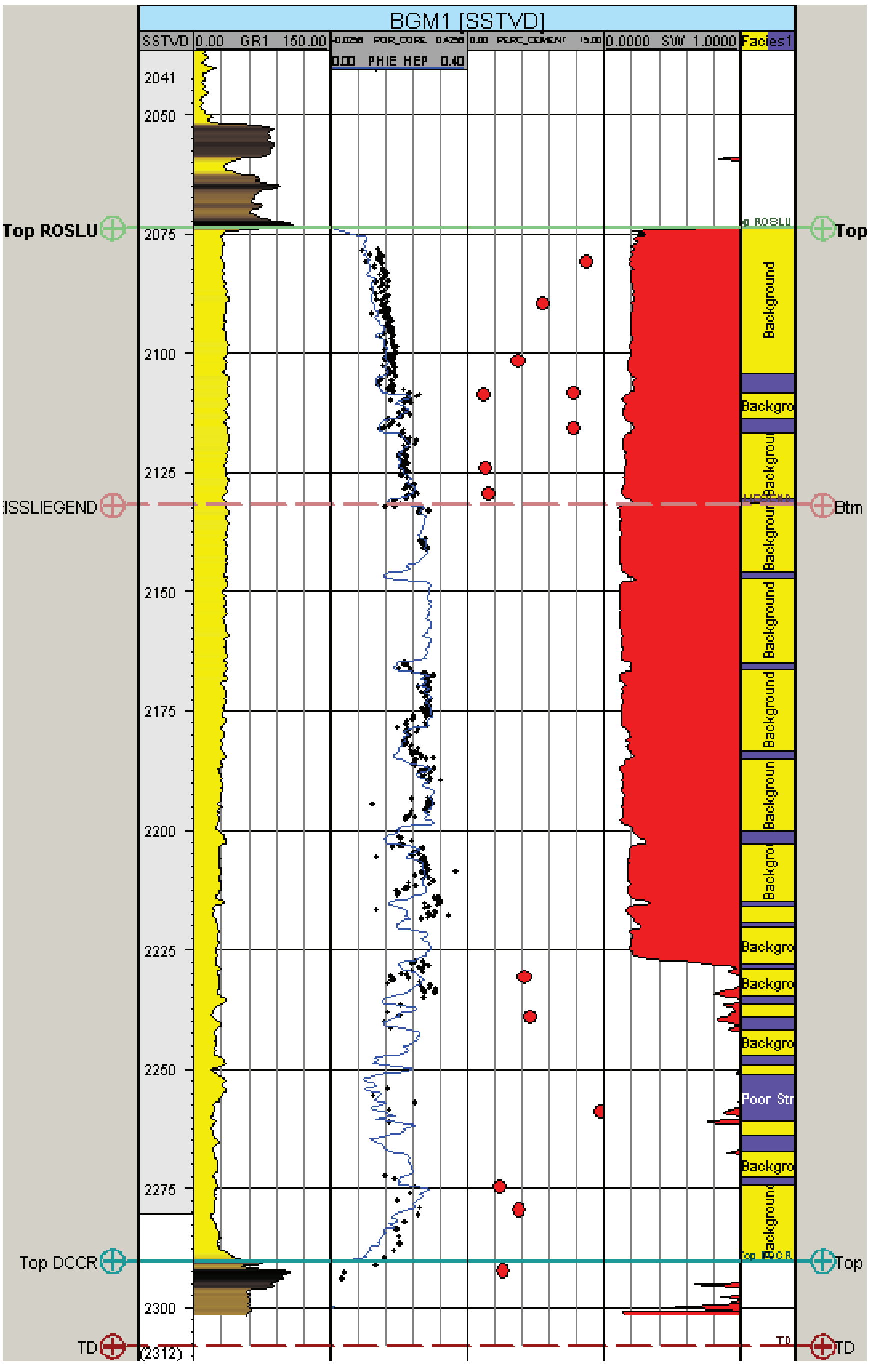

Figure 4-49 **Location of thin sections described in the petrography report. The middle Rotliegendes is unrepresented.**

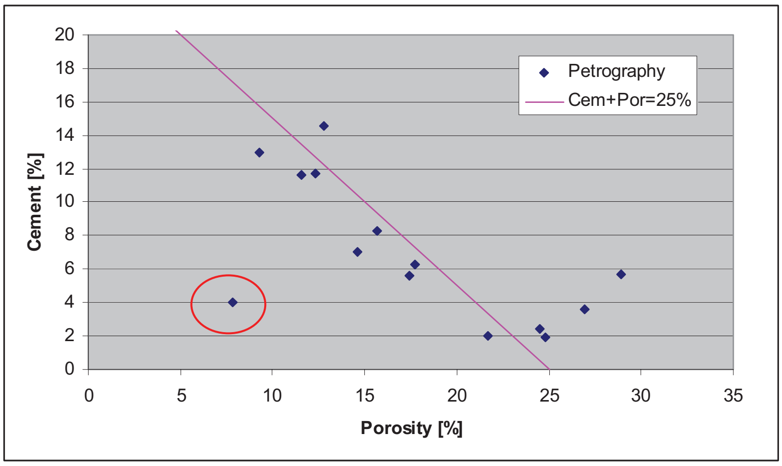

Figure 4-50 Cross-plot of cement percentage vs. porosity over the thin sections described in the petrography report. The trend plotted is for constant base porosity (25%), with varying degrees of pore-filling cement. The circled off-trend point is the bottom-most sample, which is actually taken from the Carboniferous (Figure 4-49)